IEEE Access
Multidisciplinary ⋮ Rapid Review ⋮ Open Access Journal

Received 5 February 2025, accepted 20 February 2025, date of publication 24 February 2025, date of current version 28 February 2025.

Digital Object Identifier 10.1109/ACCESS.2025.3544867

RESEARCH ARTICLE

Optimization of the Backstepping Control Parameters of an Active Electrohydraulic Suspension to Improve Passenger Comfort and Road Handling

RACHID FATTAH[1], (Member, IEEE), JEAN-PIERRE KENNE[2], KHALID BENJELLOUN[3], AND AHMED CHEBAK[1], (Senior Member, IEEE)

[1]Green Tech Institute (GTI), Mohammed VI Polytechnic University (UM6P), Ben Guerir 43150, Morocco
[2]Department of Mechanical Engineering, École de Technologie Supérieure (ÈTS), Montreal, QC H3C 1K3, Canada
[3]École Mohammadia d'Ingénieurs (EMI), Mohammed V University (UM5), Rabat 08007, Morocco

Corresponding author: Rachid Fattah (Rachid.fattah@um6p.ma)

ABSTRACT This study introduces an innovative optimization strategy for Electro-Hydraulic Active Suspension Systems (EHASS), combining game theory with Particle Swarm Optimization (PSO) to tune backstepping control parameters. Unlike conventional approaches relying on manual tuning or trial-and-error, our method systematically optimizes these parameters, ensuring a well-balanced trade-off between ride comfort and road handling. The optimization process considers worst-case road disturbances, leading to a 79.5% reduction in tracking error, a 44.7% decrease in VDV, and a 51.2% improvement in Crest Factor, complying with *ISO 2631* standards. Comprehensive validation across ten road profiles, including highly irregular terrains, confirms the robustness of the proposed method. Additionally, a comparison with Genetic Algorithm (GA)-based optimization highlights that PSO achieves superior convergence and performance. These findings establish a new benchmark for intelligent suspension control, making our approach a strong candidate for real-world automotive applications.

INDEX TERMS Electro-hydraulic active suspension, backstepping control, game theory optimization, comfort control, road handling, multi-objective optimization.

I. INTRODUCTION

Vehicle suspension systems are critical components for ensuring both road handling performance and passenger comfort [1], [2], [3]. Among these, Electro-Hydraulic Active Suspension Systems (EHASS) have emerged as a promising technology because of their ability to actively respond to road disturbances and provide superior ride quality [4], [5]. However, their inherent nonlinearities, such as fluid compressibility, varying chamber volumes, and complex valve dynamics, pose significant control challenges [6], [7]. Furthermore, recent advances in robust adaptive control have demonstrated promising results in handling actuator faults and uncertainties in EHASS [8]. These challenges necessitate advanced control strategies capable of managing such complexities.

Traditional backstepping control methods have proven effective for nonlinear systems such as EHASS [9]. However, their reliance on manual or trial-and-error parameter tuning often results in suboptimal performance and limits their applicability under diverse road conditions [10]. Recent advances in robust control design [11] and learning-based methods [12] have highlighted the potential of addressing time-varying delays, disturbances, and uncertainties. Recent studies have highlighted the potential of deep learning approaches for active suspension control [13], particularly for handling complex nonlinear dynamics and uncertain disturbances.However, while deep learning-based controllers

The associate editor coordinating the review of this manuscript and approving it for publication was Hassen Ouakad.

have demonstrated strong potential in handling nonlinear dynamics, they also come with certain limitations. These models often function as black-box systems, making stability guarantees difficult to establish [8]. In contrast, our method is built on a Lyapunov-based backstepping framework, ensuring global asymptotic stability, which is crucial for safety-critical automotive applications. Additionally, deep learning approaches require extensive training data and computational resources to generalize effectively [14]. In real-time applications, this can pose challenges due to the high inference latency and potential overfitting issues. Our approach, however, leverages offline PSO-based optimization to tune the backstepping controller parameters, allowing for real-time execution with minimal computational overhead. Another key limitation of deep learning-based methods is their sensitivity to unseen disturbances. While these controllers generalize from training data, they may struggle when exposed to unexpected road conditions [15]. Our Game-theoretic framework addresses this issue by explicitly optimizing the controller against worst-case disturbances modeled using *ISO 8608* road profiles, ensuring robustness in extreme conditions. Finally, deep learning-based controllers often require significant real-world data collection and fine-tuning before deployment [16]. In contrast, our method is fully model-based, eliminating the need for large-scale data acquisition and making it more suitable for practical deployment in automotive control systems where stability, safety, and predictability are critical. Nevertheless, most existing approaches fail to provide a systematic framework for optimizing multiple performance objectives, including tracking accuracy and compliance with the *ISO 2631* comfort standards.

Recent studies have explored various strategies for EHASS control, such as sliding mode control, adaptive control, and hybrid approaches [9], [10], [17]. However, systematic parameter optimization for backstepping control remains underexplored. This is particularly challenging because of the inherent trade-offs between road handling and passenger comfort, which require careful balancing.

Game theory provides a powerful framework for addressing such trade-offs by modeling the interaction between competing objectives as a strategic game [5], [18]. When combined with optimization techniques such as Particle Swarm Optimization (PSO), game theory offers an efficient solution to multi-objective problems in complex, nonlinear control systems [19], [20]. Furthermore, recent studies have shown the potential of combining multi-objective optimization with learning-based approaches [14], which complements our PSO-based strategy. The effectiveness of multi-objective PSO has been demonstrated in recent studies, particularly in scenarios requiring the simultaneous optimization of multiple criteria [21].

This study introduces a novel optimization strategy for EHASS that integrates game theory with PSO to optimize backstepping control parameters. Unlike conventional backstepping approaches that rely on manual tuning or heuristic adjustments [4], [9], our method systematically optimizes these parameters to enhance both ride comfort and road handling.

The proposed approach models the interaction between suspension control and road disturbances as a Game-theoretic problem, where the suspension system is optimized against worst-case road disturbances (*ISO 8608* Class H). This ensures robust performance under extreme conditions, unlike previous studies that focus on average road profiles [22], [23]. Our framework integrates tracking performance metrics with *ISO 2631* compliant comfort constraints to achieve precise road handling and enhanced passenger comfort.

This research aims to address the following key questions:

- How can game theory principles be effectively integrated with PSO to optimize backstepping control parameters?
- What optimization framework ensures robust tracking performance and compliance with the *ISO 2631* comfort standards?
- How significant are the improvements compared to conventional non-optimized control parameters?

Compared to existing methods, our main contributions include:

- **Automated optimization of backstepping parameters:** Instead of relying on manual tuning, our PSO-based optimization achieves a well-balanced trade-off between ride comfort and road handling.
- **Game-theoretic robustness:** The optimization is performed under worst-case road disturbances, making the suspension system highly robust compared to traditional methods [18], [24].
- **Extensive validation on ten road profiles:** Unlike prior works limited to two or three conditions [10], [25], our method is validated across diverse real-world driving scenarios.
- **Superior convergence and performance:** A comparison with Genetic Algorithm (GA)-based optimization demonstrates that PSO provides **faster convergence and more stable control performance** [15].

The remainder of this paper is organized as follows: Section II presents the problem formulation, including the system states, performance metrics, and control objectives. Section III introduces the road handling factors and levels, defining the RMSE-based classification used to assess suspension performance. Section IV describes the comfort factors and constraints, outlining *ISO 2631* based metrics such as RMS acceleration, Vibration Dose Value (VDV), and Crest Factor. Section V outlines the optimization approach, explaining how Particle Swarm Optimization (PSO) and Game-theoretic principles are integrated to tune the backstepping parameters. Section VI details the system modeling, covering the mechanical structure, electrohydraulic actuator dynamics, and state-space representation. Section VII presents the backstepping control strategy, including the

stability analysis and parameter selection. Section VIII discusses the simulation setup and results, including a comparative analysis with traditional approaches. Finally, Section IX concludes the paper and highlights potential directions for future research.

II. PROBLEM FORMULATION

A. NOTATION

The following notation is used throughout this paper:

1) SYSTEM STATES AND VARIABLES

- $y(t) \in \mathbb{R}^n$: State vector including positions and velocities
- $u(t) \in \mathbb{R}$: Control input voltage
- $x_r(t) \in \mathbb{R}$: Road disturbance
- $z(t)$: Vertical position output
- $f(\cdot)$, $b(\cdot)$, $h(\cdot)$: System nonlinear functions
- k_i: Backstepping control parameters

2) BACKSTEPPING CONTROL PARAMETERS

- k_i:control parameters
- e_1, e_2, e_3, e_4: Tracking errors of different system states.
- $\alpha_1, \alpha_2, \alpha_3$: Stabilizing functions used in backstepping control.
- $\psi_3(t)$, $\psi_4(t)$: Bounded nonlinear terms arising from external disturbances.
- V: Lyapunov candidate function.
- $\dot{V}$: Time derivative of the Lyapunov function.

3) PERFORMANCE METRICS

- RMSE: Root Mean Square Error
- $a_{w,\mathrm{RMS}}$: RMS acceleration
- VDV: Vibration Dose Value
- CF: Crest Factor

4) PSO ALGORITHM PARAMETERS

- ω: Inertia weight factor
- c_1, c_2: Cognitive and Social Coefficients
- r_1, r_2: Random numbers between 0 and 1
- $p_{ij}(t)$: Personal best position
- $p_{gj}(t)$: global best position
- N: Population size of the swarm.
- $\mathrm{iter}_{\max}$: Maximum number of iterations.
- $\lambda_{\mathrm{RMSE}}, \lambda_{\mathrm{RMS}}, \lambda_{\mathrm{VDV}}, \lambda_{\mathrm{Crest}}$: Weighting coefficients for the optimization cost function.
- $\mathrm{RMSE}^{\mathrm{threshold}}$: Maximum acceptable tracking error threshold.
- $a_{\mathrm{RMS}}^{\mathrm{threshold}}$: Maximum allowed RMS acceleration.
- $\mathrm{VDV}^{\mathrm{threshold}}$: Maximum allowed vibration dose value.
- $\mathrm{CF}^{\mathrm{threshold}}$: Maximum allowed Crest Factor.

5) ROAD PROFILE PARAMETERS

- PSD:Power Spectral Density
- $G_d(n)$: PSD of vertical displacement [m^3/cycle]
- n: Spatial frequency [cycles/m]
- $G_d(n_0)$: Displacement PSD at reference frequency n_0

6) HYDRAULIC SYSTEM PARAMETERS

- A_v: Valve opening area
- V_0: Oil volume in the actuator chamber
- L: Load leakage coefficient
- β: Fluid bulk modulus
- A: Actuator piston area
- τ_v: Time constant
- k: Servo-valve constant
- P_L: Differential pressure due to the load
- P_s: Source pressure
- C_d: Flow discharge coefficient
- ρ: Fluid oil density

B. GENERAL MODEL OF ACTIVE SUSPENSION SYSTEMS

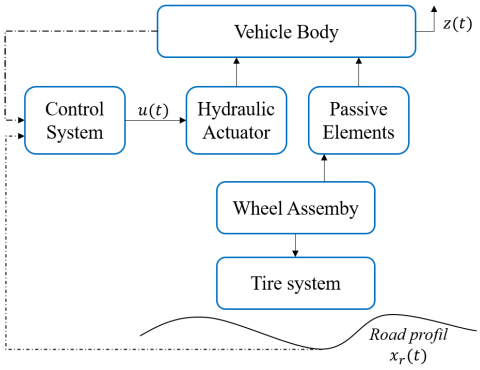

FIGURE 1. General model of an active suspension system.

We considered a general model of an active suspension system (Figure.1) based on the foundational work of [4]. The state-space representation is given by:

$$\begin{aligned} \dot{y}(t) &= f(y(t), u(t), x_r(t)) + b(y(t), t)u(t) \\ z(t) &= h(y(t)) \end{aligned} \tag{1}$$

In active suspension systems, the dynamics can be characterized by a sixth-order nonlinear system, where the state variables represent the sprung mass position (y_1) and velocity (y_2), unsprung mass position (y_3) and velocity (y_4), hydraulic pressure (y_5), and valve opening (y_6). Following this physical structure, the system can be expressed as:

$$\begin{cases} \dot{y}_1 = f_1(y) \\ \dot{y}_2 = f_2(y) \\ \dot{y}_3 = f_3(y) \\ \dot{y}_4 = f_4(y, x_r) \\ \dot{y}_5 = f_5(y) \\ \dot{y}_6 = f_6(y) + g(y)u \end{cases} \tag{2}$$

where $y = [y_1, y_2, y_3, y_4, y_5, y_6]^T \in \mathbb{R}^6$ represents the state vector, $u \in \mathbb{R}$ is the control input, x_r is the road disturbance, $f_i(\cdot)$ and $g(\cdot)$ are sufficiently smooth nonlinear functions.

C. CONTROL OBJECTIVES

The primary control objectives for the active suspension system are established based on the key literature on vehicle dynamics [1]:

- **Road Handling**: Ensure that the vehicle's body maintains a stable position relative to the road despite disturbances [1], [3].
- **Passenger Comfort Constraints**: While not directly optimized, comfort is ensured by constraining:
  -- The weighted Root Mean Square (RMS) acceleration [26]
  -- Vibration Dose Value (VDV) [26]
  -- Crest Factor [26]

  These metrics must comply with *ISO 2631* standards [26]. Recent developments in comfort-oriented control strategies have highlighted the importance of considering multiple comfort metrics simultaneously [27], which aligns with our proposed approach..
- **Control Input Saturation**: Ensure that the control input remains within the physical limits of the actuator, as discussed in [4].

D. BACKSTEPPING CONTROL STRATEGY AND OPTIMIZATION

Following the approach outlined in [4], to achieve the road handling objective, we propose a backstepping control strategy [17]. The control law takes the following form:

$$u = \phi(y, k_1, k_2, \ldots, k_m) \tag{3}$$

where $\phi : \mathbb{R}^n \times \mathbb{R}^m \to \mathbb{R}$ is a nonlinear function derived through the backstepping design procedure, $y \in \mathbb{R}^n$ is the state vector, and $k_1, k_2, \ldots, k_m$ are the positive control parameters to be optimized.

The core of our contribution lies in the optimization of the backstepping control parameters, building upon the pioneering work on Particle Swarm Optimization (PSO) by [28] and its extensions in [17] and [19]. Figure 5 illustrates the overall optimization process for the EHASS.

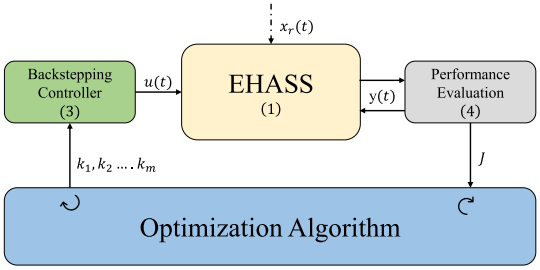

FIGURE 2. Schematic representation of the optimization process for backstepping control parameters of the EHASS.

As shown in Figure 2, we formulate this as a constrained optimization problem, following approaches similar to those discussed in [18] and [20].

$$\min_{k_1,k_2,\ldots,k_m} \text{RMSE}_{\text{handling}} \tag{4}$$

subject to: System dynamics (1)

$$\begin{aligned} &|u(t)| \le u_{\max} \quad \text{(Control input saturation)} \\ &\text{RMS}_{\text{acc}} \le \text{RMS}_{\text{threshold}} \\ &\text{VDV} \le \text{VDV}_{\text{threshold}} \\ &\text{CF} \le \text{CF}_{\text{threshold}} \\ &k_i > 0, \quad i = 1, 2, \ldots, m \end{aligned} \tag{5}$$

where:

- $\text{RMSE}_{\text{handling}}$ is the RMSE between the vehicle body position and reference trajectory, quantifying the tracking performance of the suspension system.
- $u_{\max}$ is the maximum allowable control input, representing the physical limits of the actuator.
- $\text{RMS}_{\text{threshold}}$, $\text{VDV}_{\text{threshold}}$, $\text{CF}_{\text{threshold}}$ are comfort thresholds derived from *ISO 2631* standards [26].

E. ASSUMPTIONS

To develop a realistic yet tractable control strategy, the following practical assumptions were considered:

1. **Bounded disturbances**:Road disturbances are bounded and differentiable. This assumption is physically justified by the finite nature of the road irregularities.

2. **Controllability and Observability**: The system is controllable and observable. This reflects the practical capability of the hydraulic actuator to influence the system states and the availability of reliable sensors for the position and acceleration measurements.

3. **Known Parameters**: System parameters such as spring stiffness, damping coefficients, and actuator properties are known and constant. Although real parameters may vary slightly with temperature and wear, their variation is typically minimal.

F. STABILITY ANALYSIS OF THE BACKSTEPPING CONTROL

Bechause of the cascade structure of our sixth-order system, the backstepping design focuses on the subsystem that directly affects the control objectives: the sprung mass dynamics (y_1, y_2) and the related hydraulic dynamics (y_5, y_6). This subsystem is chosen because it forms a controllable chain of integrators from the control input to the regulated output (sprung mass position), while ensuring passenger comfort and road handling performance.

The tracking errors are defined as:

- $e_1 = y_1 - y_{1ref}$: position tracking error of the sprung mass
- $e_2 = y_2 - \alpha_1$: velocity tracking error of the sprung mass
- $e_3 = y_5 - \alpha_2$: pressure tracking error
- $e_4 = y_6 - \alpha_3$: Valve opening tracking error

where α_1, α_2, and α_3 are the stabilizing functions designed using the backstepping procedure.

For this controlled subsystem, we establish the following stability theorem:

Theorem 1: For a sixth-order nonlinear system described by equation (2), under Assumptions 1-3, there exists a

backstepping control law with control gains $k_1, k_2, k_3, k_4 > 0$, such that the closed-loop system is globally asymptotically stable if the following conditions hold:

1) $k_1 > \frac{1}{2}$, $k_2 > \frac{1}{2}$,
2) $k_3 > \frac{1}{4} \max_{t\geq 0} \|\psi_3(t)\|^2$,
3) $k_4 > \frac{1}{4} \max_{t\geq 0} \|\psi_4(t)\|^2$,

where $\psi_3(t)$ and $\psi_4(t)$ represent bounded nonlinear terms that arise from the system dynamics and external disturbances.

Proof: We established the stability of the system using a backstepping design and Lyapunov analysis.

Step 1 Define the Tracking Errors: Let:

$$e_1 = y_1 - y_{1ref}, \quad e_2 = y_2 - y_{2ref}, \\ e_3 = y_5 - y_{5ref}, \quad e_4 = y_6 - y_{6ref}. \tag{6}$$

Taking their time derivatives:

$$\dot{e}_1 = \dot{y}_1 - \dot{y}_{1ref} = y_2 - \dot{y}_{1ref}. \tag{7}$$

Step 2 First Stabilizing Function: Choose the first stabilizing function:

$$y_{2ref} = -k_1 e_1 + \dot{y}_{1ref}. \tag{8}$$

Substituting y_{2ref}, we have:

$$\dot{e}_1 = -k_1 e_1 + e_2, \tag{9}$$

where $e_2 = y_2 - y_{2ref}$.

For the second error e_2, taking its derivative:

$$\dot{e}_2 = \dot{y}_2 - \dot{y}_{2ref} = f_2(y) + g_2(y)u - \dot{y}_{2ref}. \tag{10}$$

Define the second stabilizing function:

$$y_{5ref} = -e_1 - k_2 e_2 + \dot{y}_{2ref}. \tag{11}$$

Substituting y_{5ref}, we have:

$$\dot{e}_2 = -k_2 e_2 - e_1 + e_3, \tag{12}$$

where $e_3 = y_5 - y_{5ref}$.

Step 3 Third Stabilizing Function: Taking the derivative of e_3:

$$\dot{e}_3 = \dot{y}_5 - \dot{y}_{5ref} = f_5(y) - \dot{y}_{5ref}. \tag{13}$$

Define the third stabilizing function:

$$y_{6ref} = -e_2 - k_3 e_3 + \dot{y}_{5ref}. \tag{14}$$

Substituting y_{6ref}, we have:

$$\dot{e}_3 = -k_3 e_3 - e_2 + e_4 + \psi_3(t), \tag{15}$$

where $\psi_3(t)$ captures the nonlinear terms and disturbances.

Step 4 Control Law and Fourth Stabilizing Function: Taking the derivative of e_4 as:

$$\dot{e}_4 = \dot{y}_6 - \dot{y}_{6ref} = f_6(y) + g_6(y)u - \dot{y}_{6ref}. \tag{16}$$

Design the control law:

$$u = -\frac{1}{g_6(y)}\Big[k_4 e_4 + e_3 - f_6(y) + \dot{y}_{6ref}\Big], \tag{17}$$

which gives:

$$\dot{e}_4 = -k_4 e_4 - e_3 + \psi_4(t), \tag{18}$$

where $\psi_4(t)$ captures the nonlinear terms and disturbances.

Step 5 Lyapunov Function: Consider the Lyapunov candidate function:

$$V = \frac{1}{2}\sum_{i=1}^{4} e_i^2, \tag{19}$$

which is positive definite. Taking its time derivative:

$$\dot{V} = \sum_{i=1}^{4} e_i \dot{e}_i. \tag{20}$$

Substituting the error dynamics:

$$\dot{V} = e_1(-k_1 e_1 + e_2) + e_2(-k_2 e_2 - e_1 + e_3) \\ + e_3(-k_3 e_3 - e_2 + e_4 + \psi_3(t)) \\ + e_4(-k_4 e_4 - e_3 + \psi_4(t)). \tag{21}$$

Step 6 Simplification of Terms: Rearranging and grouping similar terms:

$$\dot{V} = -k_1 e_1^2 - k_2 e_2^2 - k_3 e_3^2 - k_4 e_4^2 \\ + e_3\psi_3(t) + e_4\psi_4(t). \tag{22}$$

This expression shows that the time derivative of the Lyapunov function is negative except for the terms involving $\psi_3(t)$ and $\psi_4(t)$, which represent system uncertainties.

Step 7 Applying Young's Inequality: To bound the influence of the nonlinear terms $e_3\psi_3(t)$ and $e_4\psi_4(t)$, we apply Young's inequality:

$$e_3\psi_3(t) \leq \frac{1}{4}e_3^2 + \|\psi_3(t)\|^2, \\ e_4\psi_4(t) \leq \frac{1}{4}e_4^2 + \|\psi_4(t)\|^2. \tag{23}$$

Substituting these inequalities into $\dot{V}$, we obtain:

$$\dot{V} \leq -k_1 e_1^2 - k_2 e_2^2 - k_3 e_3^2 - k_4 e_4^2 \\ + \frac{1}{4}e_3^2 + \|\psi_3(t)\|^2 + \frac{1}{4}e_4^2 + \|\psi_4(t)\|^2. \tag{24}$$

Rearranging the terms:

$$\dot{V} \leq -k_1 e_1^2 - k_2 e_2^2 - \Big(k_3 - \frac{1}{4}\Big)e_3^2 \\ - \Big(k_4 - \frac{1}{4}\Big)e_4^2 + \|\psi_3(t)\|^2 + \|\psi_4(t)\|^2. \tag{25}$$

To ensure **global asymptotic stability**, all quadratic terms must have negative coefficients. This leads to the conditions:

$$k_1 > \frac{1}{2}, \quad k_2 > \frac{1}{2}, \quad k_3 - \frac{1}{4} > 0, \quad k_4 - \frac{1}{4} > 0. \tag{26}$$

Thus, the minimum values for k_3 and k_4 are:

$$k_3 > \frac{1}{4}, \quad k_4 > \frac{1}{4}. \tag{27}$$

1) ASSUMPTIONS ABOUT $\psi_3(T)$ AND $\psi_4(T)$

To ensure stability, we assume that the nonlinear terms $\psi_3(t)$ and $\psi_4(t)$, which represent system uncertainties and external disturbances, are **bounded**. These terms are primarily influenced by:

- External road disturbances $x_r(t)$ and their derivatives $\dot{x}_r(t)$.
- Nonlinear actuator dynamics, including hydraulic pressure variations.
- Unmodeled dynamics in the suspension system.

Thus, we assume the existence of positive constants $\psi_{3,\max}$ and $\psi_{4,\max}$ such that:

$$\|\psi_3(t)\| \leq \psi_{3,\max}, \quad \|\psi_4(t)\| \leq \psi_{4,\max}, \quad \forall t \geq 0. \tag{28}$$

2) BOUNDING THE NONLINEAR TERMS AND COMPUTING K_3 AND K_4

By substituting these bounds into the Lyapunov derivative:

$$\dot{V} \leq -k_1 e_1^2 - k_2 e_2^2 - \left(k_3 - \frac{1}{4}\right) e_3^2 - \left(k_4 - \frac{1}{4}\right) e_4^2 + \psi_{3,\max}^2 + \psi_{4,\max}^2. \tag{29}$$

For $\dot{V} < 0$, we require:

$$k_3 - \frac{1}{4} > \frac{1}{4}\psi_{3,\max}^2, \quad k_4 - \frac{1}{4} > \frac{1}{4}\psi_{4,\max}^2. \tag{30}$$

Rearranging these inequalities gives the final conditions:

$$k_3 > \frac{1}{4} \max_{t \geq 0} \|\psi_3(t)\|^2, \quad k_4 > \frac{1}{4} \max_{t \geq 0} \|\psi_4(t)\|^2. \tag{31}$$

3) FINAL STABILITY CONDITION

Under these conditions:

$$\dot{V} \leq -\eta \sum_{i=1}^{4} e_i^2, \tag{32}$$

where $\eta > 0$, proving the global asymptotic stability of the closed-loop system. □

To complete the stability analysis, it is essential to verify the stability of the zero dynamics corresponding to the uncontrolled states (y_3, y_4). This analysis ensures that, while controlling the sprung mass position and the hydraulic dynamics, the unsprung mass motion remains bounded and stable.

III. ROAD HANDLING FACTORS AND LEVELS

The road handling of a vehicle is an important aspect that determines its ability to respond accurately to road disturbances and maintain stability, as discussed in [1] and [3]. This is typically evaluated using the root mean square error (RMSE) of the position, which measures the deviation of the vehicle's body position from a desired reference position.

Building on the work of [1] and [3], the RMSE in position, $\text{RMSE}_{\text{position}}$, is a statistical measure that quantifies the average deviation of a vehicle's body position from a reference position over time. This metric is important for assessing how well a suspension system maintains the desired body position in response to road disturbances. The continuous-time form of the RMSE is given by:

$$\text{RMSE}_{\text{position}} = \sqrt{\frac{1}{T}\int_0^T (y_1(t) - y_{\text{ref}}(t))^2 \, dt} \tag{33}$$

where $y_1(t)$ is the actual position of the vehicle's body at time t, $y_{\text{ref}}(t)$ is the reference position at time t, and T is the total time period over which the evaluation is performed.

Following the framework established by [1] and [3], different levels were defined based on the position RMSE.The levels are presented in Table 1.

IV. COMFORT FACTORS AND CONSTRAINTS

Passenger comfort assessment in active suspension systems is guided by several criteria outlined in the *ISO 2631* standard [26], including Weighted Root Mean Square (RMS) acceleration, Vibration Dose Value (VDV), and Crest Factor. These metrics are used as constraints in the optimization problem to ensure that the comfort levels remain within acceptable thresholds while prioritizing road handling.

A. COMFORT METRICS

1) WEIGHTED RMS ACCELERATION

The Weighted Root Mean Square (RMS) acceleration, $a_{\text{w,RMS}}$, quantifies the vibration magnitude while accounting for the frequency-dependent sensitivity of the human body to vibrations [26]. It is defined as:

$$a_{\text{w,RMS}} = \sqrt{\frac{1}{T}\int_0^T a_{\text{w}}^2(t)\, dt}, \tag{34}$$

where T is the duration of the measurement, and $a_{\text{w}}(t)$ represents the weighted acceleration signal.

2) VIBRATION DOSE VALUE (VDV)

VDV is a cumulative measure of vibration exposure over time and is particularly sensitive to high-magnitude transient vibrations.This is expressed as [26]:

$$\text{VDV} = \left(\int_0^T a_{\text{w}}^4(t)\, dt\right)^{\frac{1}{4}}. \tag{35}$$

3) CREST FACTOR

The Crest Factor evaluates the ratio of peak vibration to RMS vibration and serves as an indicator of transient shocks. This defined as [26]:

$$\text{Crest Factor} = \frac{a_{\text{w,peak}}}{a_{\text{w,RMS}}}, \tag{36}$$

where $a_{\text{w,peak}}$ is the maximum weighted acceleration.

B. COMFORT LEVELS AND THRESHOLDS

Table 2 presents the comfort levels and their corresponding thresholds based on *ISO 2631* [26]. These thresholds were used as constraints in the optimization framework to maintain acceptable passenger comfort.

TABLE 1. Quantitative definitions of road handling levels.

Handling Level	RMSE Position (m)	Description
Excellent Handling	$\text{RMSE}_{\text{position}} < 0.01$	Vehicle maintains position very close to reference under all conditions.
Good Handling	$0.01 \leq \text{RMSE}_{\text{position}} < 0.05$	Minor deviations from reference position; generally stable.
Acceptable Handling	$0.05 \leq \text{RMSE}_{\text{position}} < 0.1$	Noticeable deviations from reference but within acceptable limits.
Poor Handling	$0.1 \leq \text{RMSE}_{\text{position}} < 0.2$	Significant deviations from reference; may affect stability.
Very Poor Handling	$\text{RMSE}_{\text{position}} \geq 0.2$	Large deviations from reference; stability and control are compromised.

TABLE 2. Comfort levels and thresholds based on *ISO 2631* [26].

Comfort Level	RMS Acceleration ($a_{\text{w,RMS}}$ [m/s^2])	VDV (m/s$^{1.75}$)	Crest Factor
Very Comfortable	$a_{\text{w,RMS}} < 0.315$	VDV < 8	< 9
Comfortable	$0.315 \leq a_{\text{w,RMS}} < 0.63$	VDV ≥ 8	≥ 9
Acceptable	$0.63 \leq a_{\text{w,RMS}} < 1.0$	$9 \leq$ VDV < 10	≥ 9
Uncomfortable	$1.0 \leq a_{\text{w,RMS}} < 1.6$	$10 \leq$ VDV < 12	≥ 9
Very Uncomfortable	$1.6 \leq a_{\text{w,RMS}} < 2.5$	$12 \leq$ VDV < 15	≥ 9
Extremely Uncomfortable	$a_{\text{w,RMS}} \geq 2.5$	VDV ≥ 15	≥ 9

V. OPTIMIZATION APPROACH

The proposed optimization approach employs Particle Swarm Optimization (PSO) [28] to minimize the RMSE while respecting the constraints on the comfort and control inputs. The strategy uses five ISO road profiles (Classes D-H) to tune parameters under severe conditions and validates them across ten diverse profiles, following *ISO 2631* standards [26].

A. PARTICLE SWARM OPTIMIZATION FRAMEWORK

PSO identifies the optimal backstepping control parameters by modeling the collaborative behavior of the particles. The choice of PSO for parameter optimization is supported by recent comprehensive reviews that demonstrate its effectiveness in tuning nonlinear control systems [15].Each particle represents a solution, and its movement is determined by the velocity $v_{ij}(t)$ and position $x_{ij}(t)$ updates as follows:

$$v_{ij}(t+1) = \omega v_{ij}(t) + c_1 r_1 [p_{ij}(t) - x_{ij}(t)] + c_2 r_2 [p_{gj}(t) - x_{ij}(t)], \quad (37)$$

$$x_{ij}(t+1) = x_{ij}(t) + v_{ij}(t+1), \quad (38)$$

where c_1, c_2 are cognitive and social coefficients, and r_1, r_2 are random numbers.

B. GAME-THEORETIC OPTIMIZATION

The game theory models the interaction between the suspension controller (Player 1) and road disturbances (Player 2). Player 1 seeks to minimize tracking error while maintaining passenger comfort, whereas Player 2 represents external road disturbances that introduce unpredictable terrain variations, challenging the suspension performance.

By formulating this interaction as a **min-max optimization problem**, the controller is optimized against the most extreme disturbances, ensuring **worst-case robustness**. Instead of tuning parameters for average conditions, our approach anticipates the worst disturbances and adapts accordingly. PSO is then used to fine-tune the backstepping control parameters within this framework, optimizing the trade-off between ride comfort and road handling.

As shown in Figure 3:

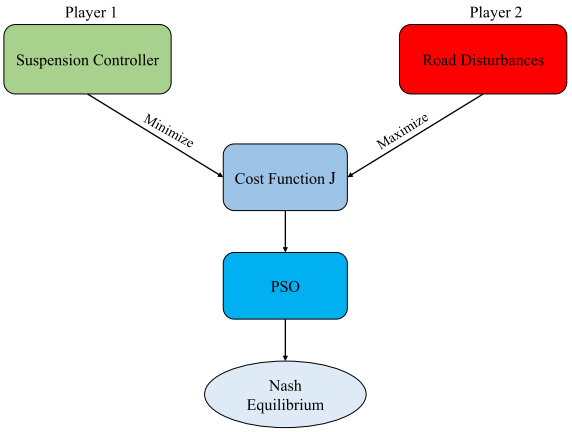

FIGURE 3. Game-theoretic min-max optimization approach.

To explicitly formalize the Game-theoretic optimization, we define the interaction as a two-player min-max problem. The suspension controller (Player 1) seeks to minimize deviations from the desired response, while the road disturbances (Player 2) act as adversarial inputs that maximize system deviations. This interaction is structured as:

$$\min_{\mathbf{k}} \max_{x_r} J(\mathbf{k}, x_r), \quad (39)$$

where $\mathbf{k} = [k_1, k_2, k_3, k_4]$ are the backstepping control parameters, and x_r represents the road disturbances modeled using *ISO 8608* profiles. The objective function $J(\mathbf{k}, x_r)$ is structured to balance tracking performance and ride comfort.By structuring the problem as a Game-theoretic min-max optimization, the backstepping parameters are optimized to ensure robustness against worst-case disturbances.

Recent research has demonstrated the effectiveness of Game-theoretic approaches in handling multiple performance objectives in active suspension systems [24], particularly when dealing with competing control objectives. This formulation ensures a Nash equilibrium in which neither player can unilaterally improve their objective without affecting the other. Therefore, the controller achieves robustness against worst-case disturbances.

C. OPTIMIZATION PHASES

1) OPTIMIZATION PHASE

The optimization used *ISO 8608* road profiles [26], characterized by their PSD:

$$G_d(n) = G_d(n_0)\left(\frac{n}{n_0}\right)^{-2}, \quad n_0 = 0.1. \tag{40}$$

Table 3 summarizes the road classifications.

TABLE 3. ***ISO 8608*** **road profile classifications.**

Class	Roughness $G_d(n_0)$ [$\mathbf{m^8}$]	Category
D	1024×10^{-6}	Poor
E	4096×10^{-6}	Very Poor
F	16384×10^{-6}	Extremely Poor
G	65536×10^{-6}	Critical
H	262144×10^{-6}	Extreme

2) VALIDATION PHASE

Validated using ten profiles,including step,sinusoidal, and random profiles, the tuned parameters where tested under various conditions (Table 4, Figure 4).

TABLE 4. **Validation road profiles.**

Profile	Key Parameters	Purpose
Step	Height: 5.4 cm	Transient Response
Smooth Wave	Amp: 2.8 cm, Freq: 0.38 Hz	Low-Frequency Response
Pothole	Depth: 5.15 cm	Impact Response
Random Wave	Amp: 2 cm, Freq: 0.1–0.8 Hz	Stochastic Response
Sinusoidal Wave	Amp: 2 cm, Freq: 0.3 Hz	Frequency Response

D. OPTIMIZATION WORKFLOW

The optimization workflow is depicted in Figure 5,which illustrates the iterative tuning and validation processes.

VI. SYSTEM MODELING

This section presents the systematic modeling approach to derive the complete state-space representation of the Electrohydraulic Active Suspension System (EHASS). Starting with the mechanical structure, we integrated the hydraulic dynamics, leading to a unified sixth-order nonlinear model that matches the general form presented in Section II. This modeling approach follows previous studies that have established detailed mathematical formulations for electrohydraulic active suspension systems [29].

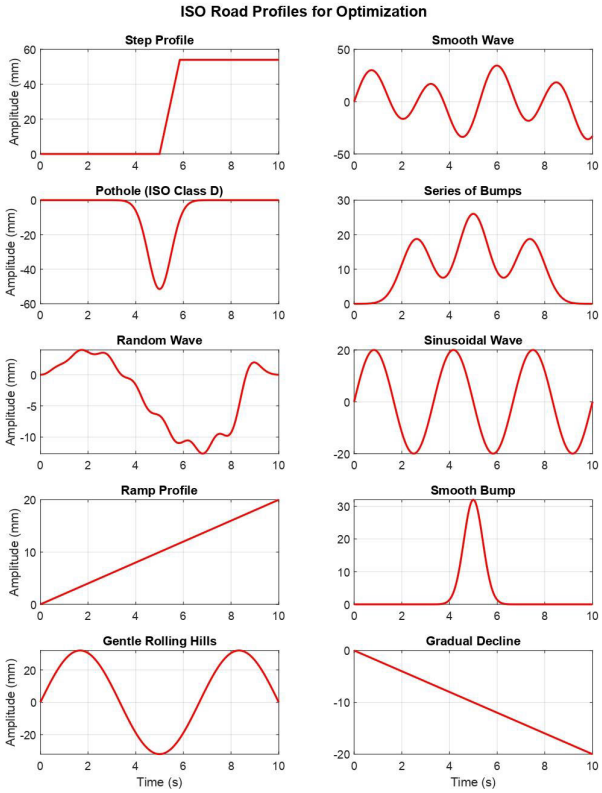

FIGURE 4. **Validation road profiles.**

A. QUARTER-CAR MECHANICAL MODEL

The quarter-car model (Figure 6) combines the following elements:

- **Passive element:** A traditional spring-damper system.
- **Active element:** A hydraulic actuator.
- **Tire model:** A parallel spring-damper configuration (Figure 7).

B. ELECTROHYDRAULIC ACTUATOR DYNAMICS

The dynamics of the electrohydraulic system are modeled based on a single-stage servo valve that controls the hydraulic actuator. The key equations are as follows:

1) SERVO VALVE DYNAMICS

$$\tau_v \dot{A}_v + A_v = ku, \tag{41}$$

2) FLOW RATE EQUATION

$$Q = C_d A_v \sqrt{\frac{P_s - P_L \operatorname{sigm}(A_v)}{\rho}}, \tag{42}$$

where the sigmoidal approximation is given by:

$$\operatorname{sigm}(A_v) = \frac{1 - \exp(-pA_v)}{1 + \exp(-pA_v)}, \quad p > 0. \tag{43}$$

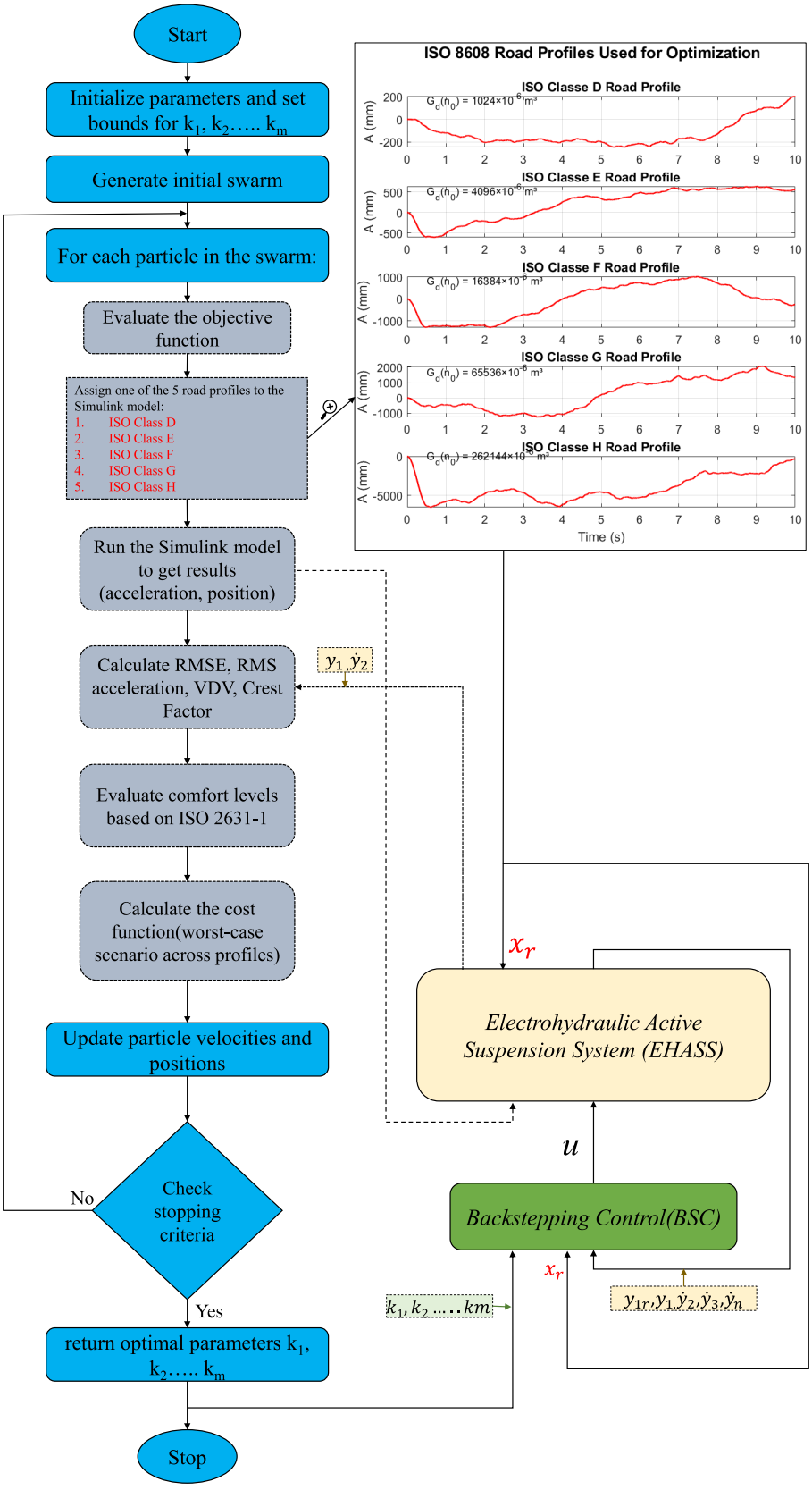

FIGURE 5. Workflow of the optimization process for backstepping control.

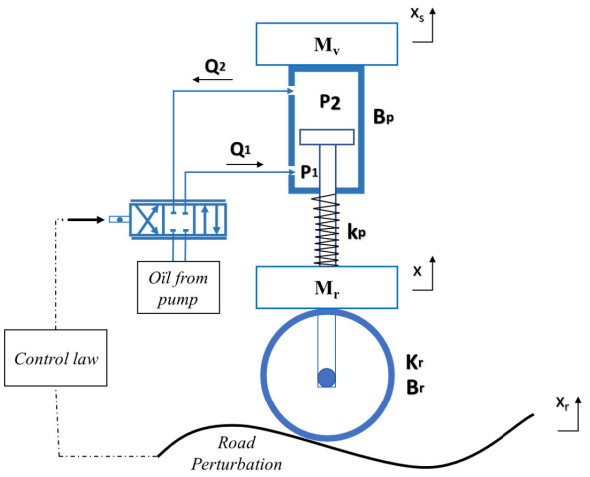

FIGURE 6. Quarter-car electrohydraulic active suspension system.

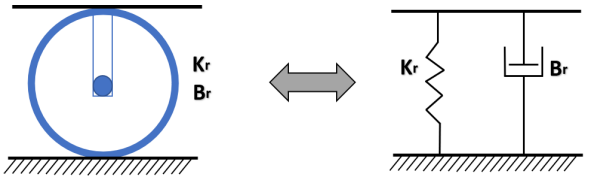

FIGURE 7. Tire model with parallel spring-damper configuration.

3) CONTINUITY EQUATION

The flow balance, accounting for the actuator motion, leakage, and fluid compressibility, is expressed as:

$$Q = C_d A_v \sqrt{\frac{P_s - P_L \text{sigm}(A_v)}{\rho}} + A(\dot{X}_s - \dot{X}) + LP_L + \dot{P}_L \frac{V_0^2 - A^2(X_s - X)^2}{2V_0\beta}. \quad (44)$$

C. VEHICLE BODY DYNAMICS

The motion of the sprung and unsprung masses is derived using Newton's laws:

1) UNSPRUNG MASS (WHEEL ASSEMBLY)

$$M_r\ddot{X} = K_p(X_s - X) + B_p(\dot{X}_s - \dot{X}) - K_r(X - X_r) - B_r(\dot{X} - \dot{X}_r) - AP_L. \quad (45)$$

2) SPRUNG MASS (VEHICLE BODY)

$$M_V\ddot{X}_s = -K_p(X_s - X) - B_p(\dot{X}_s - \dot{X}) + AP_L. \quad (46)$$

D. STATE-SPACE REPRESENTATION

Defining the state vector as:

$$y = [y_1, y_2, y_3, y_4, y_5, y_6]^T = [X_s, \dot{X}_s, X, \dot{X}, P_L, A_v]^T,$$

the complete nonlinear state-space model is:

$$\begin{aligned}
\dot{y}_1 &= y_2,\\
\dot{y}_2 &= -a(y_1 - y_3) - b(y_2 - y_4) + cy_5,\\
\dot{y}_3 &= y_4,\\
\dot{y}_4 &= d(y_1 - y_3) + e(y_2 - y_4) - f(y_3 - x_r)\\
&\quad - n(y_4 - \dot{x}_r) - hy_5,\\
\dot{y}_5 &= \frac{J}{f(y_1, y_3)}\big(c_d y_6 g(y_5, y_6)\\
&\quad + A(y_4 - y_2) - Ly_5\big),\\
\dot{y}_6 &= -\frac{1}{\tau}y_6 + \frac{k_v}{\tau}u,
\end{aligned} \quad (47)$$

where:

$$\begin{aligned}
f(y_1, y_3) &= V_0^2 - A^2(y_1 - y_3)^2,\\
g(y_5, y_6) &= \sqrt{\frac{P_s - \text{sigm}(y_6)y_5}{\rho}},\\
\text{sigm}(y_6) &= \frac{1 - \exp(-py_6)}{1 + \exp(-py_6)}.
\end{aligned} \quad (48)$$

The system parameters are given by:

$$\begin{aligned}
a &= \frac{K_p}{M_V}, \quad b = \frac{B_p}{M_V}, \quad c = \frac{A}{M_V},\\
d &= \frac{K_p}{M_r}, \quad e = \frac{B_p}{M_r}, \quad f = \frac{K_r}{M_r},\\
n &= \frac{B_r}{M_r}, \quad h = \frac{A}{M_r}, \quad J = 2V_0\beta.
\end{aligned}$$

This state-space model comprehensively captures the nonlinear dynamics of the system and, servs as the foundation for backstepping control design.

VII. BACKSTEPPING CONTROL DESIGN

The backstepping control design targets the vertical motion of the vehicle body as the primary regulated variable, directly influencing road handling and passenger comfort objectives. The tracking error for this regulated variable is defined as:

$$e_1 = y_1 - y_{1ref}. \quad (49)$$

Because of the cascaded structure of the system model, as noted by [4], where the hydraulic dynamics (y_5, y_6) directly influence the sprung mass motion (y_1, y_2), the backstepping approach is applied sequentially to this controllable subsystem.

A. CONTROL DESIGN

Step 1: Starting with the regulated variable e_1, y_2 is used as the virtual input to the subsystem $\dot{y}_1 = y_2$. Following the approach in [4], the stabilizing function, which is the desired value of y_2, is given by:

$$y_{2d} = -k_1 e_1. \quad (50)$$

Step 2: Introducing the error variable $e_2 = y_2 - y_{2d}$ and y_5 as the virtual input to the subsystem:

$$\dot{y}_2 = -a(y_1 - y_3) - b(y_2 - y_4) + cy_5, \quad (51)$$

the stabilizing function, which is the desired value of y_5, is given by:

$$y_{5d} = \alpha_0 e_1 - \alpha_1 e_2 + \alpha_2(y_2 - y_4) + \alpha_3(y_1 - y_3). \quad (52)$$

Step 3: Define the error variable as $e_3 = y_5 - y_{5d}$ and consider y_6 as the virtual input to the subsystem:

$$\dot{y}_5 = \frac{J}{V_0}\big(C_d y_6 g(.) + A(y_4 - y_2) - L y_5\big). \quad (53)$$

The stabilizing function, which determines the desired value of y_6, is expressed by:

$$y_{6d} = \frac{f(.)}{JC_d g(.)}\big[-\beta_1 e_1 - \beta_2 e_2 - \beta_3 e_3 - \gamma_1 y_1 - \gamma_2 y_2 + \gamma_3 y_3 - \gamma_4 y_4 + \gamma_5 y_5 + a_2 \dot{y}_2\big]. \quad (54)$$

Step 4: Finally, define the error variable as $e_4 = y_6 - y_{6d}$. The actual control input u is derived from the subsystem:

$$\dot{y}_6 = -\frac{1}{\tau} y_6 + \frac{k_v}{\tau} u. \quad (55)$$

The stabilizing control law u is given by:

$$u = \left(\frac{k_v}{\tau} - \frac{f(.)}{JC_d}\frac{J(.)}{g^2(.)}Y(.)\right)^{-1}\Big[-k_v e_4 + \frac{1}{\tau} y_6 - \frac{J}{f(.)} C_d g(.) e_3 - \frac{f(.)}{JC_d} Y(.)\left(\frac{H(.) - I(.)}{g^2(.)}\right) + \frac{f(.)}{JC_d g(.)} X(.) + \frac{\dot{f}(.)}{JC_d g(.)} Y(.)\Big]. \quad (56)$$

To ensure that the control law remains well-defined, the denominator in Equation (56) must be strictly nonzero. Since the system parameters k_v, τ, J, and C_d are strictly positive, the critical term:

$$D(y) = \left(\frac{k_v}{\tau} - \frac{f(.)}{JC_d}\frac{J(.)}{g^2(.)}Y(.)\right) \quad (57)$$

remains nonzero as long as $g(y)$ is bounded away from zero, which is ensured by actuator design constraints. Additionally, the nonlinear terms $f(y)$ and $Y(y)$ remain within physical limits, preventing singularities in practical operating conditions. Thus, the control law is always well-defined.

The resulting closed-loop error dynamics are:

$$\begin{aligned}
\dot{e}_1 &= -k_1 e_1 + e_2,\\
\dot{e}_2 &= -e_1 - k_2 e_2 + c e_3,\\
\dot{e}_3 &= -c e_2 - k_3 e_3 + \frac{J}{f(.)} C_d g(.) e_4 + a_2\big(f x_r + n\dot{x}_r\big),\\
\dot{e}_4 &= -\frac{JC_d g(.)}{f(.)} e_3 - k_4 e_4 - \frac{\gamma_4 f(.)}{Jc_d g(.)}\big(f x_r + n\dot{x}_r\big).
\end{aligned} \quad (58)$$

B. STABILITY ANALYSIS

The stability of the closed-loop system was verified using the results of Theorem 1. The error dynamics can be expressed as:

$$\begin{aligned}
\dot{e}_1 &= -k_1 e_1 + e_2,\\
\dot{e}_2 &= -k_2 e_2 - e_1 + e_3,\\
\dot{e}_3 &= -k_3 e_3 - e_2 + e_4 + \psi_3,\\
\dot{e}_4 &= -k_4 e_4 - e_3 + \psi_4.
\end{aligned} \quad (59)$$

Here, the terms ψ_3 and ψ_4 are identified as:

$$\psi_3 = a_2\big(f x_r + n\dot{x}_r\big), \quad (60)$$

$$\psi_4 = -\frac{\gamma_4 f(.)}{Jc_d g(.)}\big(f x_r + n\dot{x}_r\big). \quad (61)$$

From Theorem 1, cccthe following conditions for the controller gains hold:

$$k_1 > \frac{1}{2}, \quad k_2 > \frac{1}{2}, \quad (62)$$

$$k_3 > \frac{a_2^2}{4}\max_{t\geq 0}\|(f x_r + n\dot{x}_r)^2\|, \quad (63)$$

$$k_4 > \frac{1}{4}\left(\frac{\gamma_4}{Jc_d g(.)}\right)^2 \max_{t\geq 0}\|(f x_r + n\dot{x}_r)^2\|. \quad (64)$$

These conditions ensure that the Lyapunov candidate function:

$$V = \frac{1}{2}\sum_{i=1}^{4} e_i^2 \quad (65)$$

satisfies:

$$\dot{V} \leq -\eta \sum_{i=1}^{4} e_i^2, \quad (66)$$

where $\eta > 0$, which guarantees the global asymptotic stability of the error dynamics under the proposed control law.

C. ZERO DYNAMICS ANALYSIS

Because the backstepping design yields a 4th-order error dynamic while the original system is of the 6th-order, we must analyze the zero dynamics corresponding to the uncontrolled states (y_3, y_4). Setting $y_1 = e_1 = 0$, the reduced dynamics are:

$$\begin{pmatrix}\dot{y}_3\\ \dot{y}_4\end{pmatrix} = \underbrace{\begin{pmatrix}0 & 1\\ A_{03} & A_{04}\end{pmatrix}}_{M}\begin{pmatrix}y_3\\ y_4\end{pmatrix} + \begin{pmatrix}0 & 0\\ f & n\end{pmatrix}\begin{pmatrix}x_r\\ \dot{x}_r\end{pmatrix} \quad (67)$$

where:

- $A_{03} = \frac{h}{C}a - d - f$
- $A_{04} = \frac{h}{c}b - e - n$

The stability of zero dynamics is ensured by the negativity of the eigenvalues of matrix M, which completes the stability analysis of the full system.

Building on the theoretical framework and stability analysis, the following section presents the simulation tests and

TABLE 5. System parameters and optimization settings.

Category	Parameter	Symbol	Value
Backstepping	Parameter bounds	$k_i^{\min}$ $k_i^{\max}$	1 10
	Time parameters	Δt T	50 μs 10 s
PSO Settings	Population size Maximum iterations Search dimension	N $\text{iter}_{\max}$ d	50 100 4
	Cognitive coefficient Social coefficient Function tolerance	c_1 c_2 ϵ	2.0 2.0 1e-6
Objective Function Weights	RMSE weight RMS acceleration weight VDV weight Crest Factor weight	λ_{RMSE} λ_{RMS} λ_{VDV} λ_{Crest}	1 1 1 1
	RMSE penalty threshold RMS acceleration limit VDV limit Crest Factor limit	$\text{RMSE}^{\text{threshold}}$ $a_{\text{RMS}}^{\text{threshold}}$ $\text{VDV}^{\text{threshold}}$ $\text{CF}^{\text{threshold}}$	0.01 m 0.315 m/s^2 8 m/s$^{1.75}$ 9

Note: k_i represents the backstepping control parameters (k_1, k_2, k_3, k_4)

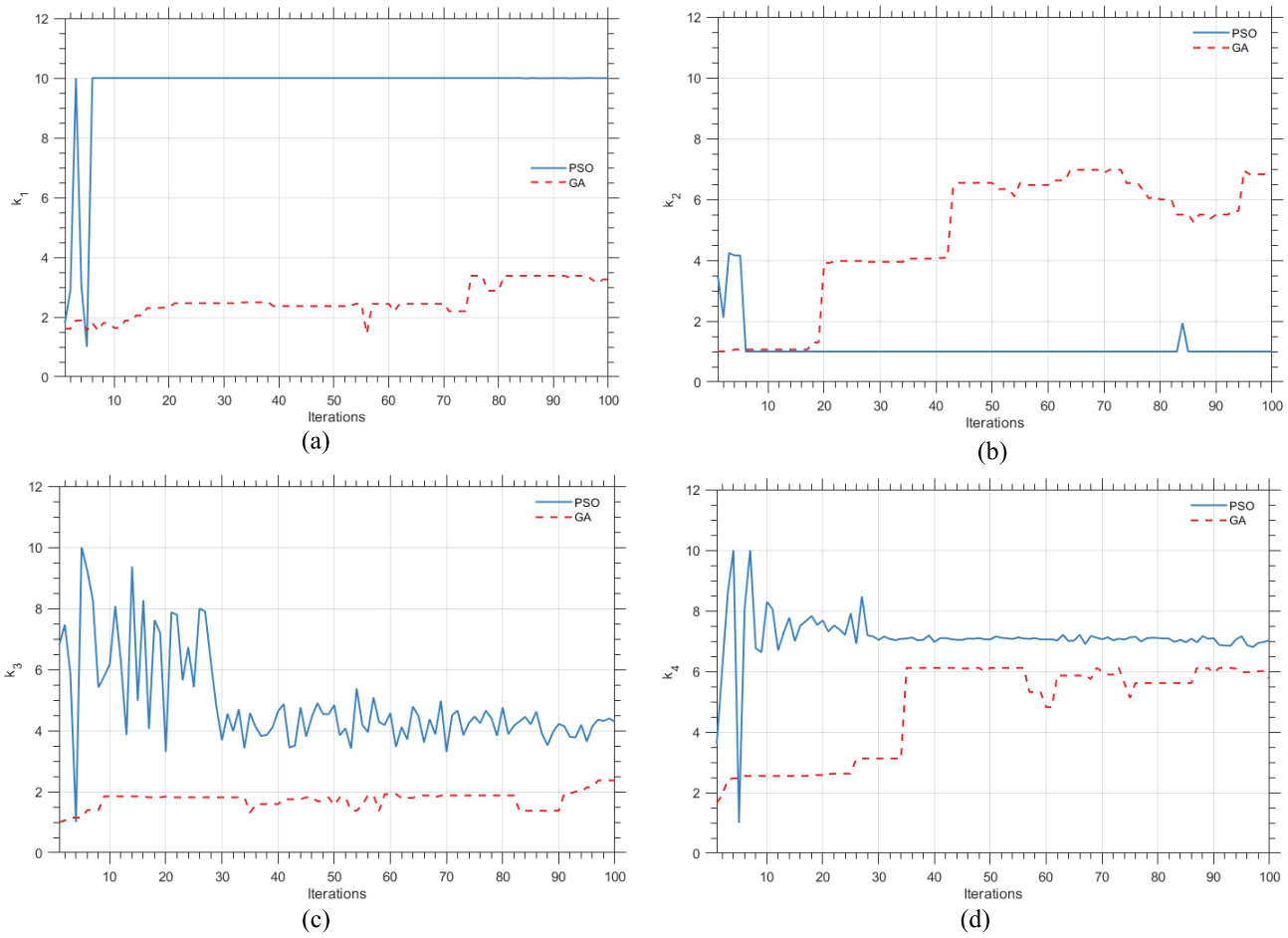

FIGURE 8. Comparative analysis of PSO and GA optimization performance for backstepping control parameters.

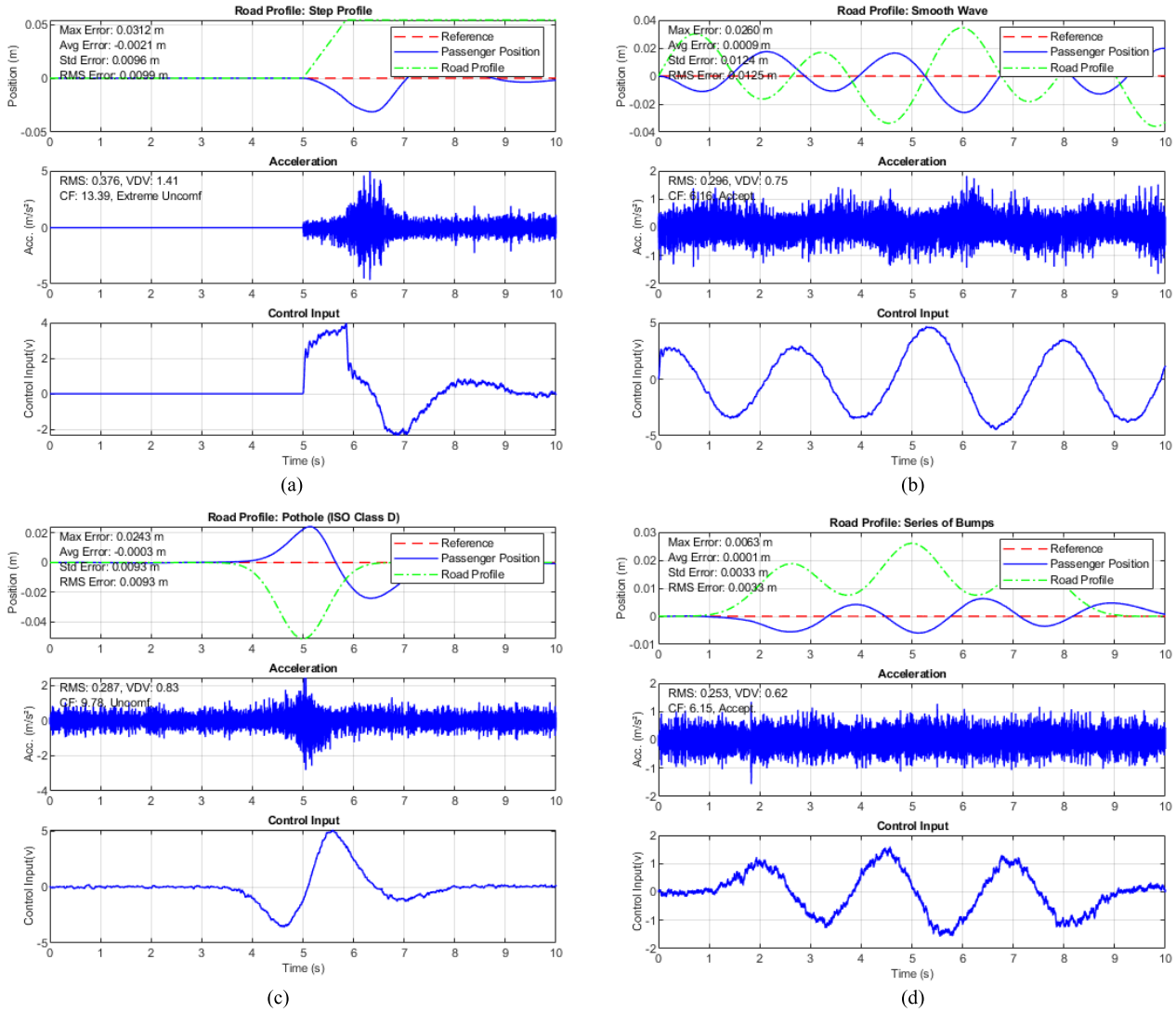

FIGURE 9. Analysis of suspension performance with non-optimized backstepping parameters under: (a) Step profile, (b) Smooth wave, (c) Pothole, (d) Series of bumps.

TABLE 6. Performance metrics of the suspension system with non-optimized parameters.

Road Profile	Max Error (m)	Avg Error (m)	Std Error (m)	RMSE (m)	RMS Acc (m/s^2)	VDV (m/s$^{1.75}$)	Crest Factor
Step Profile	0.0312	-0.0021	0.0096	0.0099	0.376	1.41	13.39
Smooth Wave	0.0260	0.0009	0.0124	0.0125	0.296	0.75	6.16
Pothole	0.0243	-0.0003	0.0093	0.0093	0.287	0.83	9.78
Series of Bumps	0.0063	0.0001	0.0033	0.0033	0.253	0.62	6.15
Random Wave	0.0072	-0.0003	0.0025	0.0028	0.259	0.63	4.94
Sinusoidal Wave	0.0148	0.0012	0.0090	0.0091	0.266	0.66	5.61
Ramp Profile	0.0014	-0.0010	0.0003	0.0010	0.254	0.63	5.46
Smooth Bump	0.0119	0.0003	0.0043	0.0044	0.244	0.61	5.36
Gentle Rolling	0.0122	-0.0008	0.0079	0.0080	0.273	0.68	5.73
Gradual Decline	0.0012	0.0009	0.0002	0.0010	0.244	0.60	5.90

optimization procedures conducted to validate and enhance the performance of the proposed optimized backstepping control strategy.

VIII. SIMULATION AND RESULTS ANALYSIS

This section is organized into multiple subsections to systematically analyze the performance of the proposed

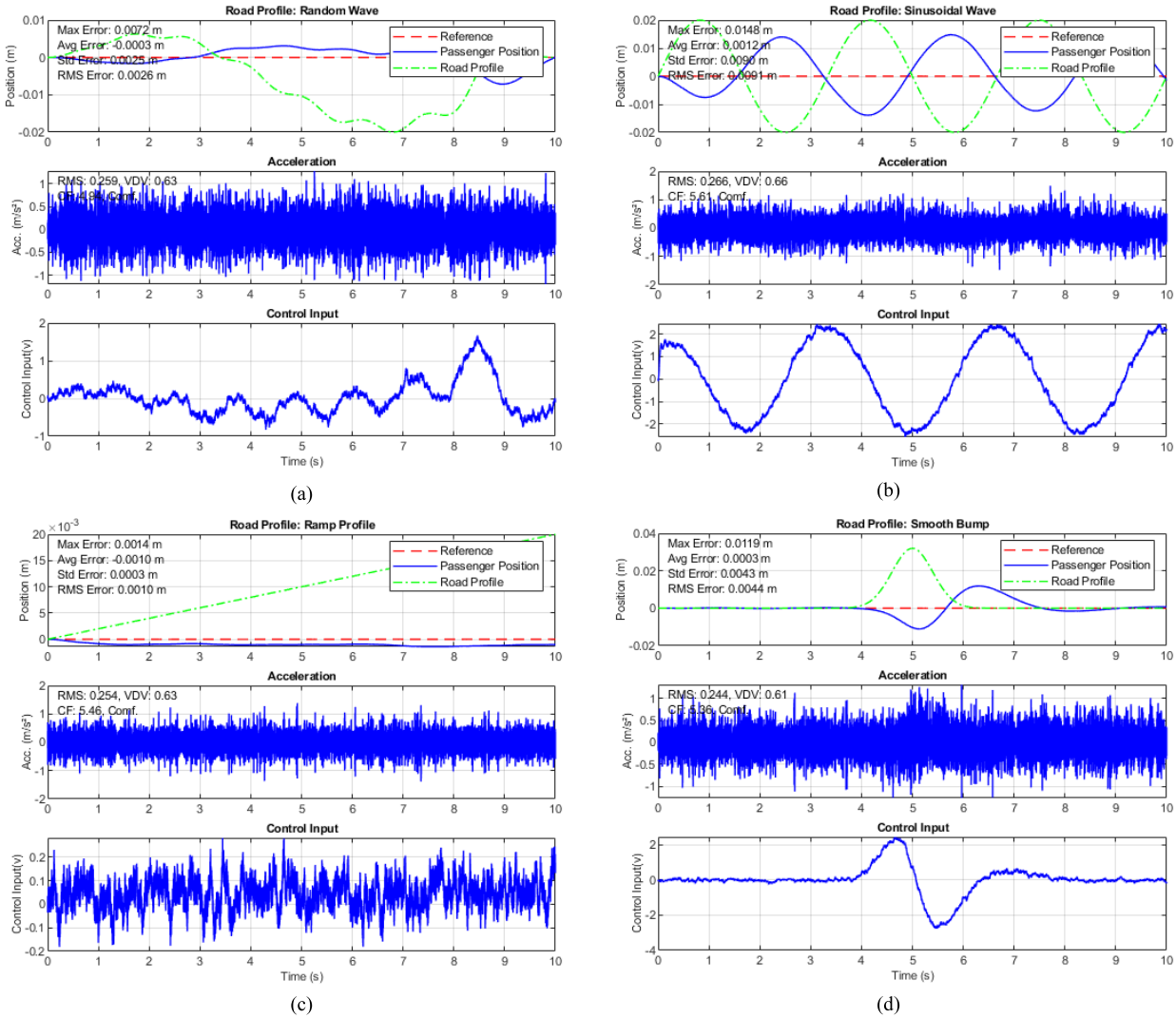

FIGURE 10. Analysis of suspension performance with non-optimized backstepping parameters under: (a) Random Wave, (b) Sinusoidal wave, (c) Ramp profile, (d) Smooth bump.

TABLE 7. Performance Metrics of the suspension system with PSO optimized parameters.

Road Profile	Max Error (m)	Avg Error (m)	Std Error (m)	RMSE (m)	RMS Acc (m/s^2)	VDV (m/s$^{1.75}$)	Crest Factor	Comfort Level
Step Profile	0.0064	-0.0003	0.0016	0.0016	0.260	0.78	6.53	Accept.
Smooth Wave	0.0053	0.0002	0.0027	0.0027	0.268	0.67	6.05	Accept.
Pothole	0.0059	0.0000	0.0019	0.0019	0.257	0.65	7.08	Accept.
Series of Bumps	0.0018	-0.0003	0.0008	0.0008	0.249	0.62	6.04	Accept.
Random Wave	0.0018	0.0000	0.0007	0.0007	0.256	0.64	5.48	Comf.
Sinusoidal Wave	0.0032	0.0001	0.0019	0.0019	0.256	0.64	6.07	Accept.
Ramp Profile	0.0004	-0.0003	0.0001	0.0003	0.249	0.61	5.70	Comf.
Smooth Bump	0.0034	-0.0000	0.0010	0.0010	0.239	0.59	6.17	Accept.
Gentle Rolling	0.0037	-0.0002	0.0022	0.0022	0.273	0.68	5.73	Comf.
Gradual Decline	0.0004	0.0003	0.0001	0.0003	0.248	0.61	5.57	Comf.

backstepping control strategy. It begins by outlining the parameter settings and simulation configurations, followed by a detailed evaluation of the optimization process using Particle Swarm Optimization (PSO). The results were then analyzed to assess the effectiveness of the controller in improving both ride comfort and road handling across various test scenarios.

A. PARAMETER SETTING

The simulation and optimization parameters are presented in Table 5. The system parameters were selected based on a validated electrohydraulic suspension design. Their detailed values are provided in **Appendix A**. The optimization settings were configured to ensure robustness and computational efficiency by tuning PSO parameters for stable

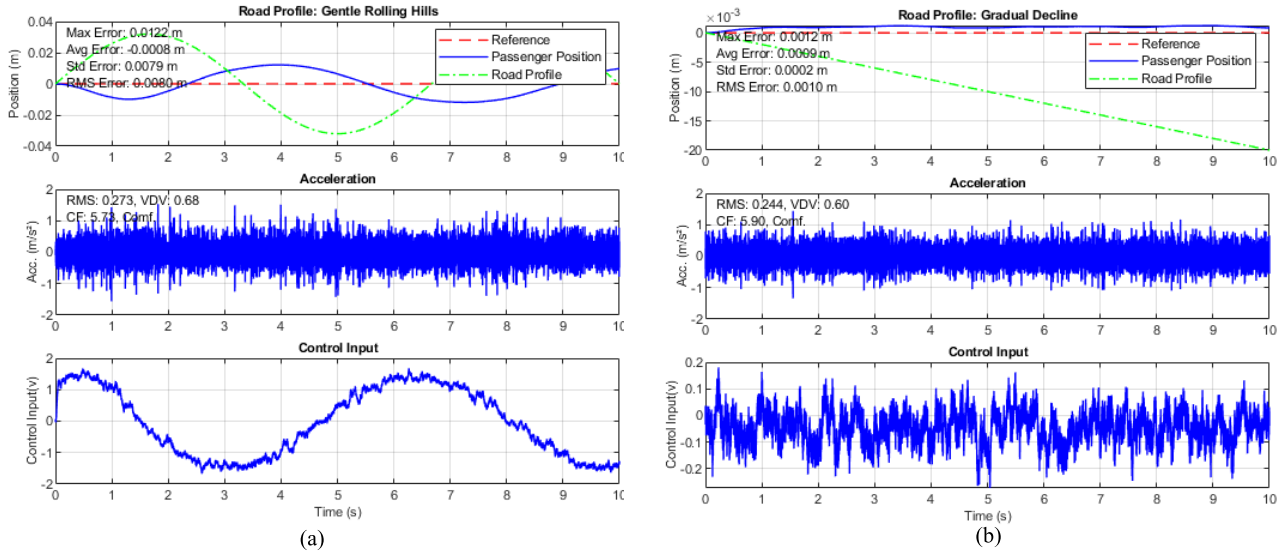

FIGURE 11. Analysis of suspension performance with non-optimized backstepping parameters under: (a) Gentle rolling, (b) Gradual decline.

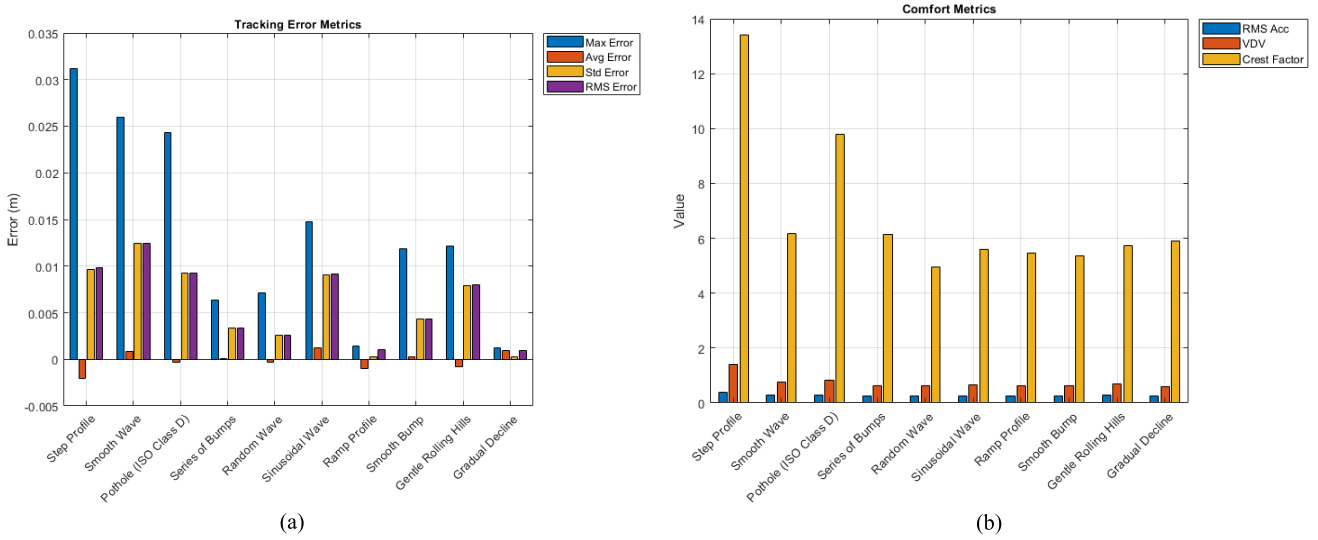

FIGURE 12. Analysis of different performance metrics with non-optimized backstepping parameters: (a) Tracking error metrics; (b) Comfort metrics.

convergence and testing under *ISO 8608* Class H road profiles.

The PSO hyperparameters were chosen based on optimization best practices. The cognitive and social coefficients ($c_1 = c_2 = 2.0$) provide a balance between exploration and exploitation, preventing premature convergence while ensuring solution stability [15], [28]. The population size ($N = 50$) and maximum iterations (100) were selected to ensure convergence within a reasonable computational time without excessive resource consumption.

Optimization Was performed using MATLAB's particle swarm optimization algorithm with the parameters specified in Table 5. The objective function evaluation combines performance criteria and comfort constraints using a min-max approach [30]to ensure robustness across all test profiles.

B. OPTIMIZATION RESULTS ANALYSIS

The optimization results depicted in Figure 8 present a comprehensive comparison between the Particle Swarm Optimization (PSO) and Genetic Algorithm (GA) for tuning the backstepping control parameters of the EHASS. The analysis revealed the significant advantages of PSO over GA in terms of convergence characteristics and solution quality.

For parameter k_1 Figure 8.a, PSO demonstrates remarkable performance by rapidly converging to an optimal value of 10 after only a few iterations, despite brief initial oscillations. In contrast, GA exhibits a much slower convergence pattern,

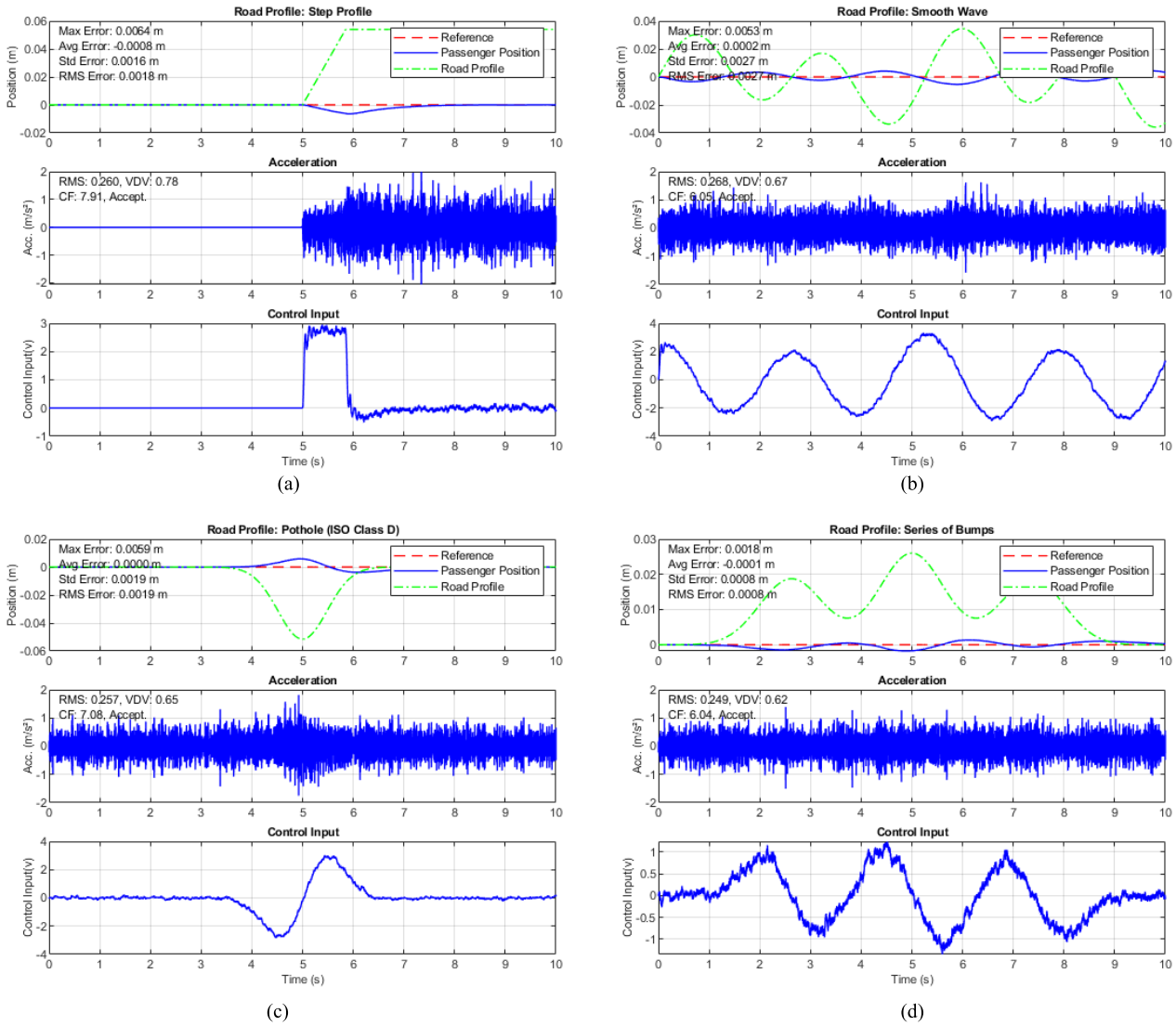

FIGURE 13. Analysis of suspension performance with PSO optimized backstepping parameters under: (a) Step profile, (b) Smooth wave, (c) Pothole, (d) Series of bumps.

gradually increasing to approximately 3.5 after 100 iterations. This substantial difference in both the convergence speed and final value highlights PSO's superior ability to escape local optima and find more optimal solutions.

The evolution of parameter k_2 Figure 8.b, shows that PSO quickly stabilizes at a lower value of approximately 1, whereas GA demonstrates a stepped increase toward higher values (approximately 6-7). PSO's ability to maintain a stable, low gain value suggests that it has identified a more efficient control configuration that could lead to a smoother system response and reduced actuator effort.

Parameter k_3 Figure 8.c, exhibits PSO's exploratory nature with initial oscillations between 4 and 10, eventually stabilizing around 4.However, GA maintains a conservative approach with values of approximately 2, showing limited exploration of the parameter space. This behavior demonstrates the PSO's capacity to thoroughly explore the solution space while still achieving a stable convergence.

The optimization of parameter k_4 Figure 8.d, further reinforces PSO's effectiveness, showing initial exploration with oscillations between 6 and 10 before settling at approximately 7, whereas GA gradually increases from 2 to 6. This pattern consistently demonstrates PSO's superior ability to explore and exploit the parameter space effectively.

The superior performance of PSO for EHASS parameter optimization can be attributed to several key factors:

1) Rapid convergence to optimal values, particularly evident in k_1 optimization
2) Enhanced exploration capabilities while maintaining convergence stability
3) Achievement of more optimal final values compared to GA

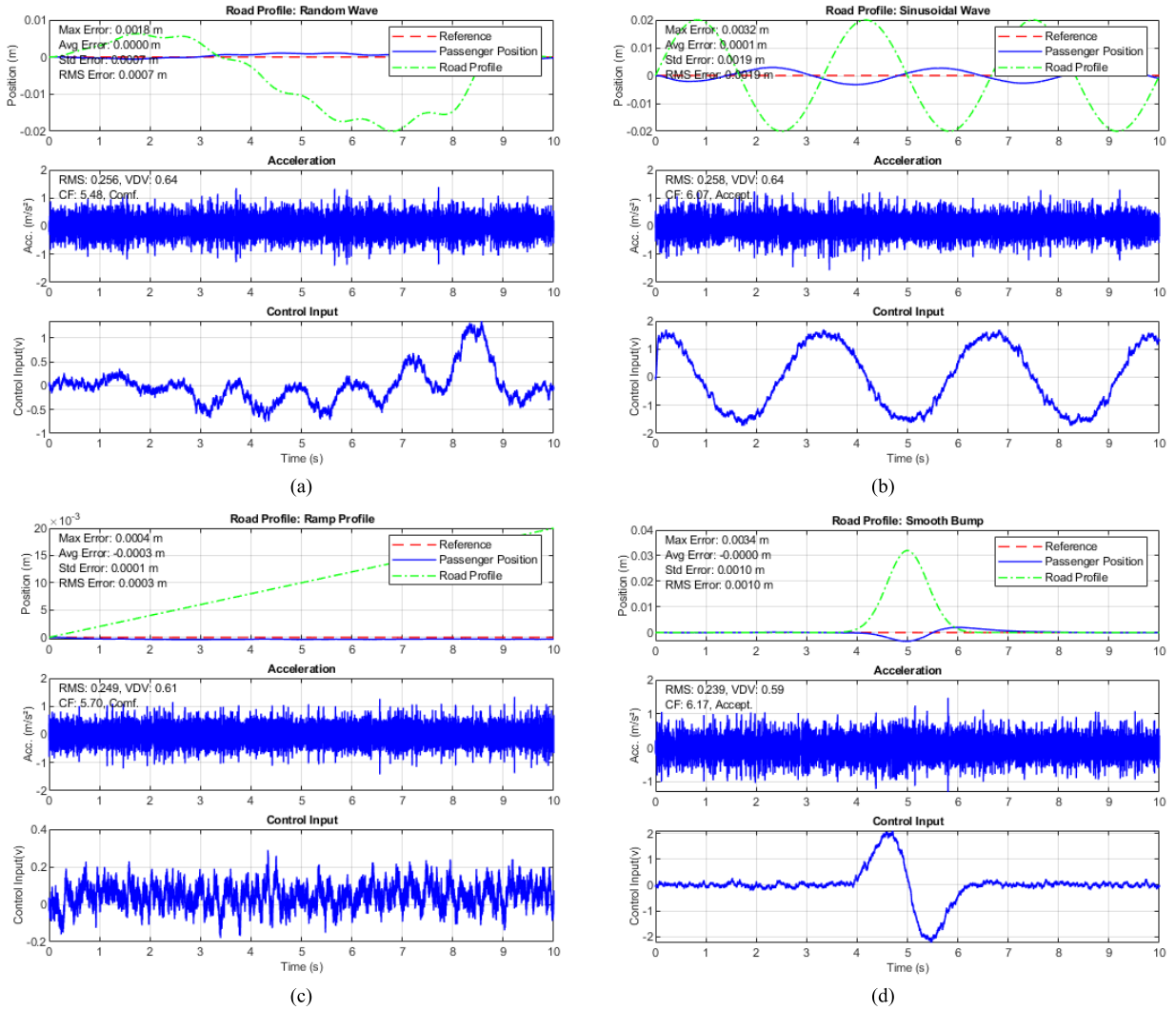

FIGURE 14. Analysis of suspension performance with PSO optimized backstepping parameters under: (a) Random wave, (b) Sinusoidal wave, (c) Ramp profile, (d) Smooth bump.

4) Efficient balance between exploration and exploitation phases

The ability to quickly identify and converge to optimal values while maintaining the flexibility to escape local optima makes PSO a more effective choice for this application than GA.Furthermore, the PSO optimization process demonstrated stable convergence behavior across multiple runs. On average, the algorithm converged within 60–80 iterations out of the 100 allowed, showing consistent parameter tuning without excessive computational cost. This confirms that the optimization approach is efficient while ensuring robustness in selecting the optimal backstepping control parameters.

C. CONTROL PERFORMANCE RESULTS ANALYSIS

The performance analysis of the backstepping controller for the EHASS demonstrated significant improvements achieved through the PSO parameter optimization. Figures 9-11 present the non-optimized controller behavior across different road profiles, with Figures 9(a-d) showing responses to step profile, smooth wave, pothole and series of bumps, Figures 10(a-d) illustrating the behavior under random waves, sinusoidal waves, ramp profiles and smooth bump disturbances, and Figures 11(a-b) depicting responses to gentle rolling and gradual decline profiles. The corresponding performance metrics are listed in Table 6.

The tracking error metrics show a remarkable improvement with PSO optimization, as shown in Figures 13-15. For the Step Profile, which represents one of the most challenging disturbances, the maximum tracking error was reduced from 0.0312m to 0.0064m (79.5% reduction), whereas the smooth wave profile showed a decrease from 0.0260m to 0.0053m (79.6% reduction). These improvements are clearly visualized in the comparative plots in Figures 12(a) and 16(a).

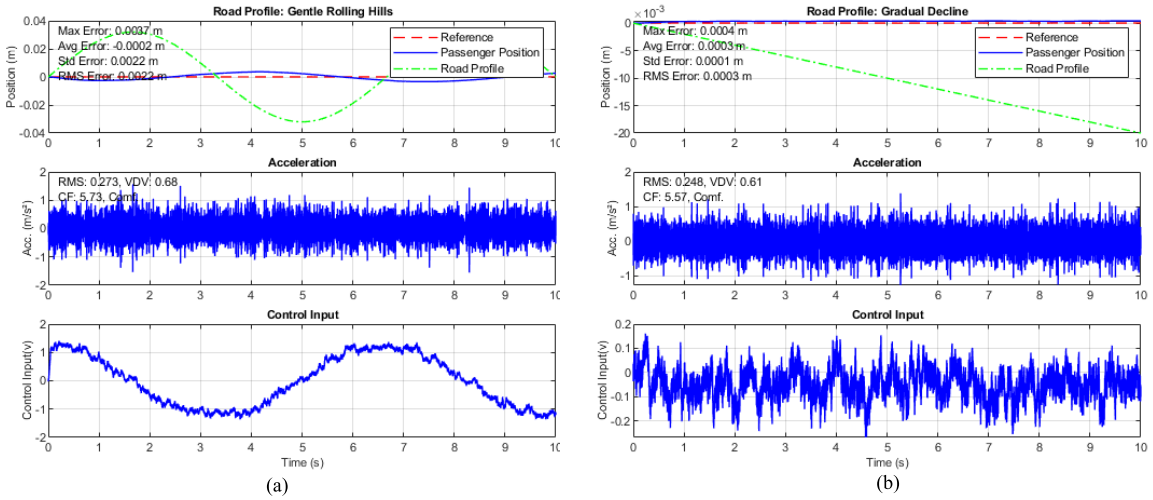

FIGURE 15. Analysis of suspension performance with PSO optimized backstepping parameters under: (a) Gentle rolling, (b) Gradual decline.

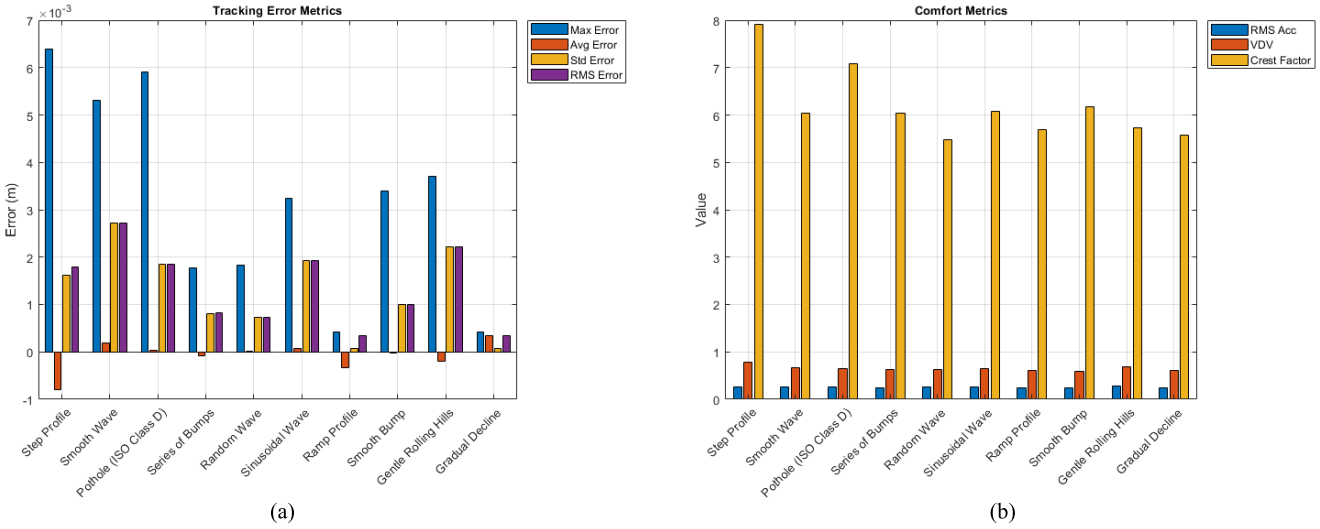

FIGURE 16. Analysis of different performance metrics with PSO optimized backstepping parameters: (a) Tracking error metrics; (b) Comfort metrics.

The comfort-related metrics demonstrate substantial enhancements between the non-optimized and optimized cases. The RMS acceleration values, particularly for the Step Profile, decreased from 0.376 m/s^2 to 0.260 m/s^2 (30.9% improvement) as shown in Table 7. The VDV saw a significant reduction from 1.41 to 0.78 (44.7% decrease) for the Step Profile, with consistent improvements across other profiles illustrated in Figures 12(b) and 16(b). The Crest Factor showed dramatic improvement, reducing from 13.39 to 6.53 for the Step Profile and from 9.78 to 7.08 for the Pothole profile.

The comfort level distribution comparison between non-optimized and optimized parameters is presented in Figure 17. Figure 17(a) shows initial varying comfort levels including "Extreme Uncomfortable" (Step Profile) and "Uncomfortable" (Pothole), while Figure 17(b) demonstrates the optimized system's achievement of either "Acceptable" or "Comfortable" ratings across all profiles. This improvement is reflected in the consistent control responses shown in Figures 13(a-d), 14(a-d), and 15(a-b),respectively.

A comprehensive performance comparison between Tables 6 and 7 validates the effectiveness of the PSO approach, demonstrating significant improvements in:

- Maximum tracking errors (average reduction over 75%)
- Tracking consistency (lower standard deviations)
- Vibration control (reduced VDV and Crest Factors)
- Comfort levels (elimination of all uncomfortable conditions)
- Disturbance handling (particularly for aggressive profiles)

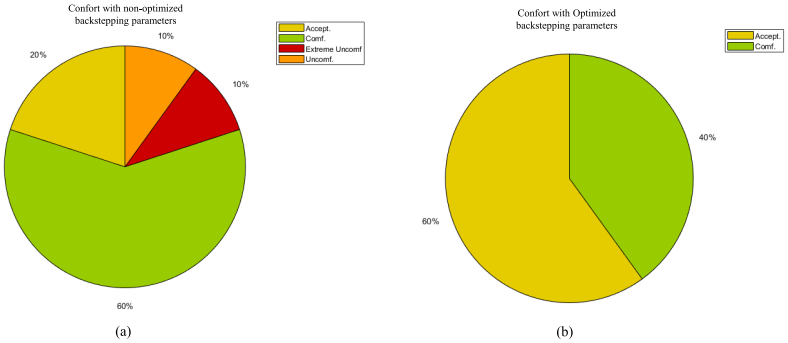

FIGURE 17. Comfort level distribution comparison between non-optimized and optimized backstepping parameters.

These results confirm the PSO-optimized controller's ability to achieve a superior balance between tracking performance and ride comfort, particularly evident in its handling of aggressive disturbances while maintaining passenger comfort. The consistent improvement across all metrics and road profiles, as documented throughout Figures 9-17, demonstrates the robustness of the PSO-optimized solution for EHASS control applications.

This study has made significant contributions to the optimization and control of Electro-Hydraulic Active Suspension Systems (EHASS). By leveraging Particle Swarm Optimization (PSO) within a Game-theoretic framework, the study achieved notable improvements in tracking accuracy, ride comfort, and overall system stability under various road conditions. The results demonstrate reductions in tracking and significant enhancements in comfort metrics, including vibration dose values and crest factors. These advancements highlight the robustness and adaptability of the proposed control strategy,which makes it a promising solution for real-world applications in advanced suspension systems. Furthermore, the compliance of the approach with *ISO 2631* standards ensures its relevance for automotive industries aiming to develop next-generation intelligent suspension technologies, offering improved safety and passenger comfort.

IX. CONCLUSION

This study introduced a novel optimization strategy for backstepping control parameters in Electro-Hydraulic Active Suspension Systems, integrating game theory principles with Particle Swarm Optimization. The proposed approach addresses the fundamental challenge of simultaneously optimizing road handling and passenger comfort while overcoming the limitations of traditional parameter tuning methods.

The obtained results demonstrate significant improvements over conventional approaches, with the PSO-optimized controller achieving a **79.5% reduction in maximum tracking error for step profiles** and a **44.7% decrease in vibration exposure**. The game theory framework effectively manages the inherent trade-off between road handling and passenger comfort, successfully eliminating all instances of "uncomfortable" ride conditions while maintaining excellent tracking performance. Furthermore, comparative analysis with Genetic Algorithm (GA) optimization confirms the superior convergence characteristics of the PSO-based approach, achieving optimal parameters in fewer iterations while maintaining better stability.

It should be noted that this study assumes constant system parameters, without considering parametric uncertainties that might affect real-world performance. Additionally, while the current approach ensures asymptotic stability, it does not guarantee finite-time or fixed-time convergence, which could be crucial for certain automotive applications requiring strict temporal performance bounds.

Furthermore, the proposed method has some limitations that should be acknowledged:

- **Dependence on Accurate System Modeling:** The controller assumes known system parameters, which may vary in real-world applications.
- **Computational Cost:** The PSO-based optimization requires multiple iterations, making real-time implementation challenging.
- **Lack of Experimental Validation:** The current study is simulation-based, and future work will also focus on the experimental validation of the proposed approach using a real electrohydraulic suspension system. This will allow us to assess its real-world performance, particularly in terms of robustness, actuator dynamics, and computational feasibility in practical applications.
- **Extreme Uncertainties:** While the approach is robust against disturbances, its performance under severe uncertainties (e.g., actuator faults) requires further analysis.

Despite the computational cost of PSO, it is important to note that the optimization is performed **offline** to determine the optimal backstepping control parameters. In real-time applications, the controller operates using **pre-optimized

fixed parameters**, requiring only algebraic calculations, which ensures computational efficiency.

These findings align with recent advances in active suspension control while offering novel contributions through the Game-theoretic PSO approach.

Future research should address the current limitations of this study by exploring several advanced control objectives. One promising direction is the development of adaptive versions of the proposed control scheme to manage parametric and time-varying uncertainties effectively. Another important avenue involves the integration of finite-time control techniques to ensure convergence within specified time bounds, particularly for applications that require strict temporal performance. Furthermore, extending the methodology to fixed-time stability frameworks would enhance its robustness by enabling convergence independent of the initial conditions. Finally, the experimental validation of physical systems is crucial for evaluating the robustness and practicality of the proposed approach under real-world uncertainties and disturbances. Although the framework developed in this study has demonstrated significant improvements in suspension control, it also provides a strong foundation for addressing these advanced challenges in future work.

APPENDIX A
SYSTEM VARIABLES

The following table provides the key system variables and their respective values used in the model of the electrohydraulic active suspension system (EHASS):

Symbol	Parameter	Value
M_v	Actuator mass	40 kg
M_r	Tire mass	32 kg
x_r	Perturbation	20 cm
B_p	Passive suspension damping	800 N·s/m
K_p	Passive suspension rigidity	16,812 N/m
B_r	Tire damping coefficient	800 N·s/m
K_r	Tire stiffness	190,000 N/m
β	Bulk modulus	7.995×10^8 N/m^2
L	Leakage coefficient	9.047×10^{-13} m^5/N·s
P_s	Supply pressure	500 psi
A_V	Valve opening area	20.2683×10^{-4} m^2
V_0	Volume of actuator	195.37×10^{-6} m^3
ρ	Fluid oil density	857 kg/m^3
τ_v	Time constant	0.0035 s
k	Servo-valve constant	1.3714×10^{-6} m^2/V
A	Actuator piston area	20.2683×10^{-4} m^2
C_d	Flow discharge coefficient	0.63
p	Sigmoid function	2000

APPENDIX B
CONTROLLER PARAMETERS

The following table presents the controller parameters for the backstepping control design, showing both non-optimized and optimized values:

Parameter	Non-Optimized Value	Optimized Value
k_1	2.01	9.99
k_2	1.56	1.00
k_3	1.45	3.65
k_4	1.95	6.75

REFERENCES

[1] L. Zhang, J. Wang, and W. Li, "Vehicle dynamics control: State-of-the-art and future perspectives," *IEEE Trans. Veh. Technol.*, vol. 72, no. 5, pp. 5123–5138, May 2023.
[2] F. Zhao, J. Zhang, and H. Wang, "Intelligent control strategies for vehicle active suspension systems: A survey," *IEEE/CAA Journal of Autom. Sinica*, vol. 10, no. 4, pp. 860–877, Apr. 2023.
[3] S. Xu, H. Li, and J. Wang, "Adaptive robust control of active suspension systems with event-triggered scheme," *IEEE Trans. Ind. Electron.*, vol. 70, no. 9, pp. 9234–9245, Sep. 2023.
[4] C. Kaddissi, J.-P. Kenne, and M. Saad, "Drive by wire control of an electro-hydraulic active suspension a backstepping approach," in *Proc. IEEE Conf. Control Appl., (CCA)*, Aug. 2005, pp. 1581–1587.
[5] B. Yang, W. Li, and L. Zhang, "Active suspension control using deep reinforcement learning: A comprehensive review," *IEEE Trans. Neural Netw. Learn. Syst.*, vol. 34, no. 5, pp. 2123–2138, May 2023.
[6] Y. Liu, W. Chen, and R. Wang, "Adaptive sliding mode control for active suspension systems with actuator saturation," *IEEE Trans. Ind. Electron.*, vol. 70, no. 9, pp. 9234–9245, Sep. 2023.
[7] F. Zhao, H. Wang, and J. Zhang, "Neural network adaptive control for active suspension systems with input saturation," *IEEE Trans. Neural Netw. Learn. Syst.*, vol. 34, no. 7, pp. 6923–6934, Jul. 2023.
[8] R. Wang, W. Chen, and H. Gao, "Robust $h\infty$ control for active suspension systems with actuator faults and time delays," *IEEE Trans. Syst., Man, Cybern., Syst.*, vol. 53, no. 5, pp. 3156–3167, Sep. 2023.
[9] B. Shaer, J.-P. Kenné, C. Kaddissi, and C. Fallaha, "A chattering-free fuzzy hybrid sliding mode control of an electrohydraulic active suspension," *Trans. Inst. Meas. Control*, vol. 40, no. 1, pp. 222–238, Jan. 2018.
[10] A. M. Al Aela, J.-P. Kenne, and H. Angue Mintsa, "A novel adaptive and nonlinear electrohydraulic active suspension control system with zero dynamic tire liftoff," *Machines*, vol. 8, no. 3, p. 38, Jul. 2020.
[11] Y. Liu, W. Li, H. Zhang, and L. Chen, "Robust $h\infty$ control of active suspension systems with time-varying delays and disturbances," *IEEE Access*, vol. 11, pp. 31245–31256, 2023.
[12] W. Chen, Z. Liu, and Y. Wang, "Learning-based control for active suspension systems: A deep reinforcement learning approach," *IEEE Access*, vol. 11, pp. 42156–42167, 2023.
[13] W. Zhang, X. Li, and H. Du, "Deep learning-based active suspension control: A survey," *IEEE Trans. Neural Netw. Learn. Syst.*, vol. 34, no. 8, pp. 4245–4261, Aug. 2023.
[14] Y. Chen, Z. Liu, and W. Chen, "Multi-objective optimization of active suspension systems using reinforcement learning," *IEEE/ASME Trans. Mechatronics*, vol. 28, no. 3, pp. 1523–1534, Jun. 2023.
[15] M. Liu, Y. Zhang, and X. Wang, "Particle swarm optimization-based parameter tuning for nonlinear control systems: A comprehensive review," *IEEE Access*, vol. 11, pp. 54321–54338, 2023.
[16] W. Sun, H. Zhang, and Y. Luo, "Adaptive neural control for nonlinear active suspension systems with input saturation," *IEEE Access*, vol. 11, pp. 18956–18967, 2023.
[17] L. Wu, D. Zhao, X. Zhao, and Y. Qin, "Nonlinear adaptive backstepping optimization control of the hydraulic active suspension actuator," *Processes*, vol. 11, no. 7, p. 2020, Jul. 2023.
[18] S. Chen, W. Li, and L. Zhang, "Game-theoretic optimal control for active suspension systems under multiple objectives," *IEEE Trans. Control Syst. Technol.*, vol. 31, no. 2, pp. 878–889, Jul. 2023.
[19] J. Li, Y. Liu, and W. Zhang, "Multi-objective optimization of active suspension control using improved particle swarm algorithm," *Mech. Syst. Signal Process.*, vol. 188, Sep. 2023, Art. no. 109821.
[20] J. Wu, Z. Wang, and N. Zhang, "Optimization-based control allocation for over-actuated active suspension systems," *Mech. Syst. Signal Process.*, vol. 185, Aug. 2023, Art. no. 109523.
[21] J. Li, G. Yang, W. Zhang, and Y. Liu, "Optimization-based control strategy for active suspension systems using multi-objective particle swarm optimization," *IEEE Access*, vol. 11, pp. 47123–47134, 2023.

[22] W. Sun, H. Li, and B. Yang, "Active suspension control with integrated preview strategy and model predictive approach," *IEEE Trans. Veh. Technol.*, vol. 72, no. 1, pp. 843–855, Feb. 2023.
[23] J. Wang, B. Yang, and W. Li, "Nonlinear model predictive control for active suspension systems with preview information," *IEEE Trans. Control Syst. Technol.*, vol. 30, no. 6, pp. 2534–2545, Oct. 2022.
[24] R. Wang, H. Zhang, and J. Wang, "Game-theoretic optimization for active suspension with multiple performance objectives," *IEEE Trans. Control Syst. Technol.*, vol. 31, no. 4, pp. 1678–1689, Apr. 2023.
[25] Y. Huang, J. Na, and X. Wu, "Output feedback control of active suspension systems with experimental validation," *IEEE Trans. Ind. Electron.*, vol. 69, no. 11, pp. 11456–11466, Nov. 2022.
[26] "Mechanical vibration and shock-evaluation of human exposure to whole-body vibration," ISO 2631-1:1997, Tech. Rep., Sep. 2023.
[27] K. Li, W. Chen, and Y. Liu, "Comfort-oriented control of active suspension systems: Recent advances and future trends," *IEEE Trans. Ind. Electron.*, vol. 70, no. 11, pp. 11234–11245, Nov. 2023.
[28] J. Kennedy and R. C. Eberhart, "Particle swarm optimization," in *Proc. Int. Conf. Neural Netw. (ICNN)*, vol. 4, Nov. 1995, pp. 1942–1948.
[29] R. Fattah, J.-P. Kenne, K. Benjelloun, and A. Chebak, "Comparative analysis of reaching laws in sliding mode control for electrohydraulic active suspension systems under complex road trajectories," in *Proc. 7th Int. Conf. Mechatronics, Robot. Autom. (ICMRA)*, Sep. 2024, pp. 1–9.
[30] S. Chen, W. Li, and L. Zhang, "Event-triggered control of active suspension systems with network constraints," *IEEE Trans. Ind. Electron.*, vol. 70, no. 2, pp. 2234–2245, Oct. 2023.

RACHID FATTAH (Member, IEEE) received the M.Sc. degree in mechanical engineering from the École Mohammadia d'Ingénieurs (EMI), Rabat, Morocco, in 2021, and the Aggregation degree in industrial sciences, in 2022. He is currently pursuing the Ph.D. (by research) degree with the Green Tech Institute (GTI), Mohammed VI Polytechnic University (UM6P), Ben Guerir, Morocco. He was an Education Fellow with GTI, UM6P. His research interests include the design and control of electrohydraulic suspension systems, advanced control techniques, and optimization methods, such as game theory and particle swarm optimization (PSO) to enhance road handling and passenger comfort. He focuses on the development of innovative solutions in automotive engineering and control systems.

JEAN-PIERRE KENNE received the bachelor's degree in mechanical engineering from the University of Douala, Cameroon, in 1984, and the M.Sc. and Ph.D. degrees in mechanical engineering from Polytechnique Montréal, Canada, in 1991 and 1998, respectively.

In 1999, he was a Project Manager with the Digital Control System Department, GEBO Canada. In 2000, he joined the Department of Mechanical Engineering, École de Technologie Supérieure (ÉTS), Montreal, where he currently teaches courses in control theory, fluid power systems, and the design and control of manufacturing systems. He is also a Professor with the Department of Mechanical Engineering and the Director of the Laboratory of Integrated Production Technologies. His research interests include control theory, capacity planning, control of manufacturing systems, and optimization of production systems.

KHALID BENJELLOUN received the State Engineer degree from the École Mohammadia d'Ingénieurs (EMI), Rabat, Morocco, in 1987, and the M.Sc.A. and Ph.D. degrees in mechanical engineering from Polytechnique Montréal, Montreal, QC, Canada, in 1993 and 1996, respectively.

In 1989, he joined EMI, where he is currently a Professor teaching control theory, nonlinear control systems, and robotics. He is also an affiliated Professor with the Green Tech Institute (GTI), Mohammed VI Polytechnic University (UM6P), Ben Guerir, Morocco. His research interests include advanced, intelligent, nonlinear, and stochastic control systems, with applications in industrial processes, robotics, and systems with nonlinear and random dynamics.

AHMED CHEBAK (Senior Member, IEEE) received the M.Sc. and Ph.D. degrees from Laval University, Canada, and the Engineering Diploma degree in electromechanics from the National School of Mineral Industry, Rabat, Morocco. He has been a Professor of electrical engineering with Mohammed VI Polytechnic University, Morocco, since 2019, and the Director of the Green Tech Institute. He was a Full Professor with the University of Quebec at Rimouski, Canada, and a Research Associate and a Lecturer with Laval University. His research interests include smart energy management, electric and hybrid vehicle traction system optimization, and electric machine design.